lines, UAS-*Caz*-IR$_{180-346}$) of *Drosophila* Caz, respectively. The RNAi of the fly strain obtained from the VDRC (w; UAS-*Caz*-IR$_{363-399}$; +) was targeted to the region corresponding to residues 363–399 of *Drosophila* Caz (UAS-*Caz*-IR$_{363-399}$).

Reportedly, *Caz* mRNA and Caz protein are enriched in the central nervous system (CNS), and Caz protein is present in eye imaginal discs (27). To efficiently screen for genes that affect the phenotypes caused by *Caz*-knockdown, we generated model flies with eye-specific *Caz*-knockdown. Specific knockdown of *Caz* in eye imaginal discs was achieved by crossing the transgenic flies carrying a UAS-*Caz*-IR, in which *Caz* dsRNA is expressed, with *GMR-GAL4* driver lines (*GMR-GAL4*; UAS-*Caz*-IR/+; +). Phenotypes of those model flies are easily characterized by abnormal rough eye morphology; scanning electron microscope (SEM) images showed fusion of ommatidia and loss of mechanosensory bristles (Fig. 1). Phenotypes of those fly lines carrying each UAS-*Caz*-IR crossed with the *GMR-GAL4* driver strain are summarized in Table 1. Flies carrying *GMR-GAL4*; +; + alone exhibited apparently normal eye morphology (Fig. 1A; *GMR*). Flies carrying *GMR-GAL4*; UAS-*Caz*-IR$_{1-167}$/+; + (GMR>UAS-*Caz*-IR$_{1-167}$) and those carrying *GMR-GAL4*; UAS-*Caz*-IR$_{363-399}$/+; + (GMR> UAS-*Caz*-IR$_{363-399}$) showed essentially the same rough-eye phenotype (Fig. 1B and C). These results demonstrated that the rough-eye phenotype observed in *Caz*-knockdown flies was not due to a possible insertional mutation or off-target effect, but rather to reduced Caz protein levels. Throughout the following studies, we used fly strains carrying UAS-*Caz*-IR$_{363-399}$, and UAS-*Caz*-IR hereafter refers to this fly strain.

Loss-of-function mutations and overexpression of *ter94* conversely modified the compound eye degeneration induced by *Caz*-knockdown

To examine a genetic interaction between *Caz* and ALS-causing genes, we first crossed eye-specific *Caz*-knockdown flies with several fly lines carrying different mutations in various ALS-causing genes, and their progeny were screened for eye phenotypes. From these screens, we detected a genetic interaction between *Caz* and *ter94*, the *Drosophila* ortholog of human *VCP*. We crossed *Caz*-knockdown flies with ethyl methanesulfonate-induced *ter94* mutations, $ter94^{K15502}$ and $ter94^{03775}$. The phenotypic characterization of two P-element alleles of *ter94* mutations was described previously (28). According to this report, female germ-line clones of a strong loss-of-function allele of *ter94*, $ter94^{K15502}$, do not produce germaria or egg chambers, and female germ-line clones of another slightly less strong loss-of-function allele of *ter94*, $ter94^{03775}$, formed germalia which give rise to stage 6 or 7 egg chambers before degeneration occurs (28). From these findings, we used the $ter94^{K15502}$ mutation as a strongest loss-of-function allele and the $ter94^{03775}$ mutation as a strong loss-of-function allele. The strongest ($ter94^{K15502}$) and strong ($ter94^{03775}$) loss-of-function mutations in the heterozygous states remarkably enhanced the rough-eye phenotype induced by eye-specific *Caz*-knockdown GMR>UAS-*Caz*-IR$_{363-399}$/ $ter94^{K15502}$ (Fig. 1D) and GMR>UAS-*Caz*-IR$_{363-399}$/ $ter94^{03775}$ (Fig. 1E), respectively. The progeny of eye-specific *Caz*-knockdown flies became lethal at the pupal stage when crossed with *ter94*-knockdown or a chromosomal deficiency line: *Df (2R) X1* lacking the genomic region 46C2-47A01 that contains *ter94*. These results indicate that loss-of-function mutations of *ter94* act as dominant enhancers of the *Caz*-knockdown-induced rough-eye phenotype. Conversely, the overexpression of wild-type *ter94* (GMR>UAS-*Caz*-IR$_{363-399}$/ UAS-*ter94*) obviously suppressed the rough-eye phenotype induced by eye-specific *Caz*-knockdown (Fig. 1G) based on a comparison with the responder control of UAS-*ter94* flies (GMR>UAS-*Caz*-IR$_{363-399}$/UAS-*GFP*) (Fig. 1F).

Loss-of-function mutation and overexpression of *ter94* had opposite effects on nuclear Caz signals in the larval CNS

We demonstrated in our previous paper that *Drosophila* Caz was strongly expressed in the CNS of third instar larvae and localized in the nucleus (19). Therefore, we investigated whether neuron-specific *Caz*-knockdown changed the expression or subcellular localization of Caz or both; specifically, we crossed fly lines carrying UAS-*Caz*-IR with *elav-GAL4* driver lines. To monitor Caz expression and localization, we immunostained brain-ventral ganglia complexes (BVGCs) of third instar larvae with anti-Caz antibody, which was developed previously (19), and quantified the immunofluorescent signals. The BVGCs of the control larvae, which carried w; +; *elav-GAL4/+* (*elav/+*), exhibited ubiquitous signals of endogenous Caz (Fig. 2, a driver control, A1), but the signal intensity of endogenous Caz in the BVGCs was remarkably reduced in neuron-specific *Caz*-knockdown larvae carrying UAS-*Caz*-IR/+; *elav-GAL4/+* (Fig. 2, elav>UAS-*Caz*-IR, C1). In driver control larvae, anti-Caz immunoreactivity was evident in the nucleus of the neuronal cells, but it did not colocalize with actin filaments stained with phalloidin (Fig. 2, B1, B2, B1+B2) or with chromosomes stained with diamino-2-phenylidole (DAPI; Fig. 2, B1, B3, B1+B3). These findings indicated that Caz must localize in the nucleoplasm. The intensity of nuclear Caz signals was significantly reduced in the BVGCs of neuron-specific *Caz*-knockdown larvae carrying elav>UAS-*Caz*-IR [intensity units = 8.89 (arbitrary units), measured in Fig. 2, D1] compared with that of driver control larvae (intensity units = 31.5, measured in Fig. 2, B1; $P < 0.001$, Fig. 2G).

Next, we examined the effects of ter94 on neuron-specific *Caz*-knockdown with regard to Caz levels and localization. First, we examined Caz expression and localization in larvae carrying a heterozygous loss-of-function *ter94* mutation and neuron-specific *Caz*-knockdown constructs. Larvae carrying the strongest loss-of-function allele of *ter94* and neuron-specific *Caz*-knockdown, UAS-*Caz*-IR/ $ter94^{K15502}$; *elav-GAL4/+* (Fig. 2, elav>UAS-*Caz*-IR/$ter94^{K15502}$, E1) exhibited remarkably reduced Caz signals in the BVGCs when compared with UAS-*Caz*-IR/+; *elav-GAL4/+* larvae. The intensity of nuclear Caz signal was significantly reduced in these larvae carrying elav>UAS-*Caz*-IR/$ter94^{K15502}$ (intensity units = 6.68, measured in Fig. 2, F1), even compared with that of the larvae carrying elav>UAS-*Caz*-IR (Fig. 2, D1) ($P < 0.05$, Fig. 2G). These results indicated that neuron-specific *Caz*-knockdown significantly reduced nuclear Caz expression, and this reduction was enhanced by genetic crossing with the strongest loss-of-function allele of *ter94*.

Conversely, compared with the Caz signals in BVGCs of larvae carrying UAS-*Caz*-IR/UAS-*GFP*; *elav-GAL4/+* (Fig. 3, elav>UAS-*Caz*-IR/UAS-*GFP*, A1), Caz signals in

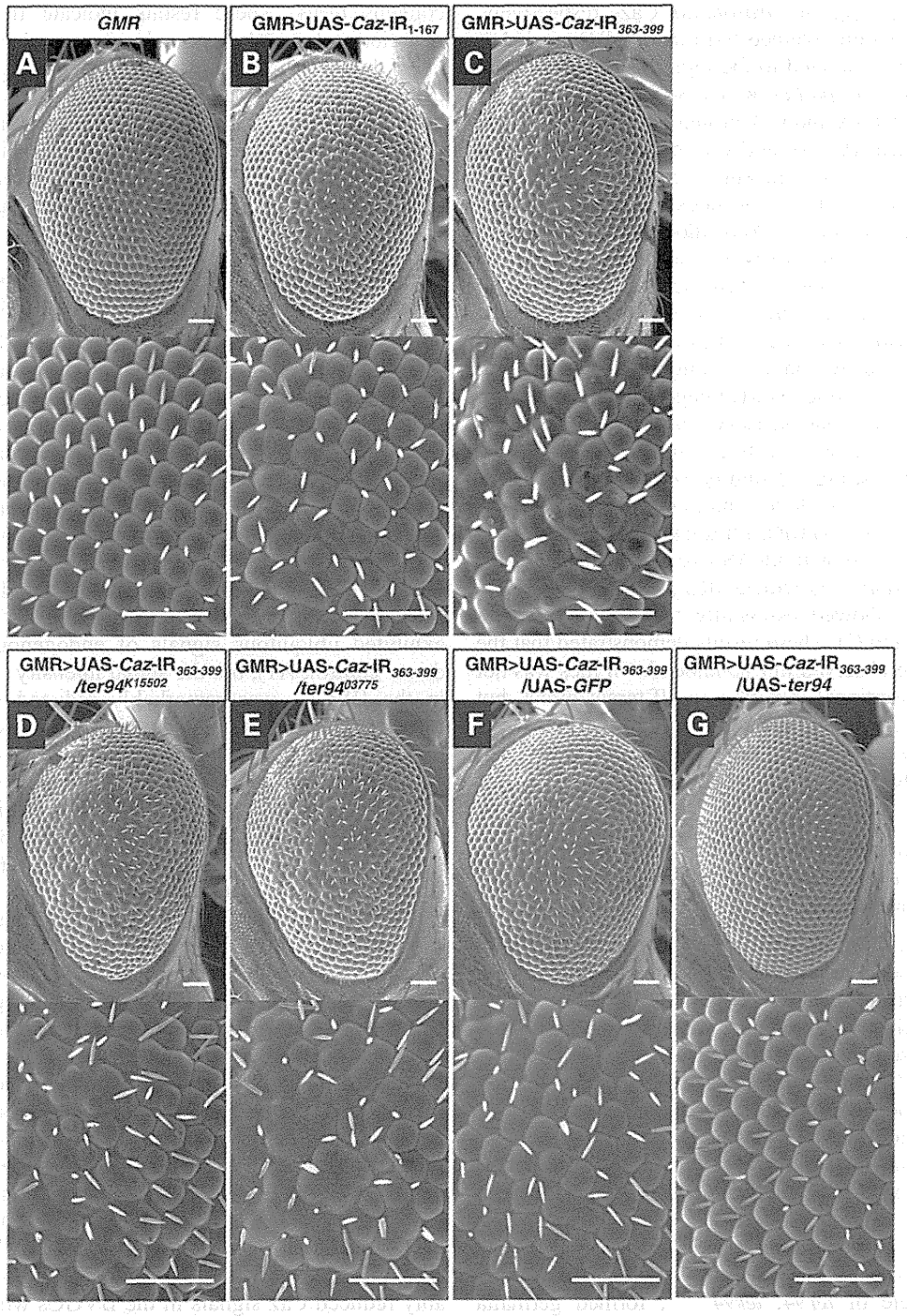

Figure 1. The rough-eye phenotype induced by *Caz*-knockdown is modified by genetic changes in *ter94*. Each panel shows a scanning electron micrograph of the compound eye of a 3-day-old adult fly. Each lower panel is a higher magnification image of the corresponding upper panel. Specific knockdown of *Caz* in eye imaginal discs was achieved by crossing the transgenic flies that carried UAS-*Caz*-IR with the *GMR-GAL4* driver. (**A**) The eyes of a control fly carrying *GMR-GAL4*; +; + (*GMR*) exhibit apparently normal eye morphology having an organized ommatidial architecture. (**B** and **C**) Adult eyes from two independent fly lines with eye-specific *Caz*-knockdown. Flies from line with UAS-*Caz*-IR1–167 (strain 4, Table 1) or from the line with UAS-*Caz*-IR363–399 were crossed with flies from the *GMR-GAL4* driver strain. Resultant flies carrying GMR>UAS-*Caz*-IR1–167 (B) or GMR>UAS-*Caz*-IR363–399 (C) have essentially the same rough-eye phenotype and exhibit ommatidial degeneration. (**D** and **E**) Adult eyes from two independent fly lines; each line has eye-specific *Caz*-knockdown and a distinct loss-of-function mutation in *ter94*. The eye-specific *Caz*-knockdown fly line (GMR>UAS-*Caz*-IR363–399/UAS-*Caz*-IR363–399) was crossed with flies carrying the strongest ($ter94^{K15502}$) or a strong ($ter94^{03775}$) loss-of-function *ter94* mutation. The resultant flies carrying GMR>UAS-*Caz*-IR363–399/$ter94^{K15502}$ (D) or GMR>UAS-*Caz*-IR363–399/$ter94^{03775}$ (E) show rough-eye phenotypes that is enhanced relative to that observed in flies with GMR>UAS-*Caz*-IR363–399 alone (C). Adult eyes from fly lines resulting from crosses of eye-specific *Caz*-knockdown flies with UAS-*GFP* (GMR>UAS-*Caz*-IR363–399/UAS-*GFP*, a responder control, **F**) or UAS-*ter94* (GMR>UAS-*Caz*-IR363–399/UAS-*ter94*, **G**). The rough-eye phenotype induced by eye-specific *Caz*-knockdown is obviously less severe in the presence of UAS-*ter94* (G) than in the presence of UAS-*GFP* (F). Posterior is to the right, and dorsal is to the top. The flies were developed at 28°C. Scale bars indicate 50 μm.

BVGCs were remarkably stronger in larvae carrying UAS-*Caz*-IR/ UAS-*ter94*; *elav-GAL4/+*, in which wild-type *ter94* was overexpressed under the *Caz*-knockdown background (Fig. 3, elav>UAS-*Caz*-IR/UAS-*ter94*, C1). Quantification of the Caz signal revealed that the intensity of nuclear Caz signal was 3.69-fold higher in elav>UAS-*Caz*-IR/UAS-*ter94* larvae (intensity units = 23.5, measured in Fig. 3, D1) than in elav> UAS-*Caz*-IR/UAS-*GFP* larvae (intensity units = 6.36, measured in Fig. 3, B1; $P < 0.001$, Fig. 3E). These results indicated that overexpression of wild-type *ter94* restored the reduced Caz signal in the nucleus induced by neuron-specific *Caz*-knockdown. Taken together, our presented results suggest that ter94 levels could enhance or rescue the Caz-knockdown phenotype.

To clarify whether or not altered ter94 protein levels affect the knock-down machinery, we carried out immunoblot analyses of CNS extracts of third instar larvae carrying *elav/+*, elav>UAS-*Caz*-IR, elav>UAS-*Caz*-IR/*ter94* ^{K15502}, elav>UAS-*Caz*-IR/UAS-*GFP* and elav>UAS-*Caz*-IR/UAS-*ter94*. A single major band with an apparent molecular weight of 45 kDa was detected on immunoblots of all the flies using the anti-Caz antibody (Supplementary Material, Fig. S1A). The intensity of this Caz protein band was apparently reduced in larvae carrying elav>UAS-*Caz*-IR compared with its intensity in larvae carrying *elav/+* (Supplementary Material, Fig. S1A and B). We then found that there was no apparent difference in Caz protein levels of CNS extracts either between the larvae carrying elav>UAS-*Caz*-IR and elav>UAS-*Caz*-IR/*ter94*^{K15502} or between the larvae carrying elav>UAS-*Caz*-IR/UAS-*GFP* and elav>UAS-*Caz*-IR/UAS-*ter94* (Supplementary Material, Fig. S1A and B). These results suggest that ter94 levels do not affect the Caz protein level on *Caz*-knockdown larvae, but indeed decrease or restore nuclear Caz protein levels in *Caz*-knockdown larvae.

Effects of a loss-of-function mutation and of overexpression of *ter94* on the mobility defects caused by neuron-specific *Caz*-knockdown

Because ALS is an age-related motor neuron disease, we examined the effect of neuron-specific *Caz*-knockdown on the locomotive function of adult flies of different ages by using a well-established climbing assay (29). We also examined the effects of loss-of-function or overexpression of *ter94* on changes in climbing ability caused by neuron-specific *Caz*-knockdown. All the fly strains showed an age-dependent decline in the climbing ability (Fig. 4). Neuron-specific *Caz*-knockdown flies carrying elav>UAS-*Caz*-IR exhibited a significantly decreased climbing ability at the following days of age; day 7, −10.4%; and day 21, −16.8%, $P < 0.001$; day 14, −10.6%, $P < 0.01$; day 28, −14.7%, $P < 0.05$ (Fig. 4A, gray columns). Flies carrying the strongest loss-of-function allele of *ter94* and neuron-specific *Caz*-knockdown (elav>UAS-*Caz*-IR/*ter94*^{K15502}) had significantly worse locomotive ability than did flies with neuron-specific *Caz*-knockdown alone (elav>UAS-*Caz*-IR) for every age examined (day 3, −14.0%; day 7, −19.5%; day 14, −35.2%; day 21, −49.7%; day 28, −63%; $P < 0.001$, Fig. 4A, black columns). Conversely, flies that overexpressed wild-type *ter94* in the background of neuron-specific *Caz*-knockdown (elav>UAS-*Caz*-IR/UAS-*ter94*) had significantly better climbing ability than did control flies with neuron-specific *Caz*-knockdown (elav>UAS-*Caz*-IR/UAS-*GFP*) until day 14 (day 3, +24.8%; day 14, +21.8%, $P < 0.001$; day 7, +15.5%, $P < 0.01$; Fig. 4B, black columns), but not after that (day 21, not significant, $P = 0.98$; day 28, reduced climbing ability, −37.4%, $P < 0.01$; Fig. 4B, black columns). There were no significant differences in climbing abilities among *elav/+* (a driver control), UAS-*Caz*-IR/+ (a responder control) and *ter94* ^{K15502}/+ flies in each day after exclusion that was monitored until 14 days (Supplementary Material, Fig. S2). Flies carrying elav>UAS-*Caz*-IR/UAS-*GFP* exhibited a significantly decreased climbing ability for every age examined (day 3, −32.8%; day 7, −23.8%; day14, −26.1%; day 21, −42.4%; day 28, −47.9%, $P < 0.001$; Fig. 4B, gray columns) compared with those carrying *elav/+* (Fig. 4B, white columns). Until day 3, the climbing ability of flies carrying elav>UAS-*Caz*-IR/UAS-*ter94* was recovered almost as well as that of flies carrying *elav/+*. However, that of flies carrying elav>UAS-*Caz*-IR/UAS-*ter94* was not fully recovered, and significantly less than that of those carrying *elav/+* after day 3 at the following days of age; day 7, −12.8%; day 21, −42.4%; day 28, −27.8%, $P < 0.001$; day 14, −10.0%, $P < 0.01$ (Fig. 4B, black columns) compared with those carrying *elav/+* (Fig. 4B, white columns). Together, our data demonstrate that neuron-specific *Caz*-knockdown leads to a severe progressive locomotive defect in adult flies, and that overexpression of wild-type *ter94* could rescue the locomotive defect until certain fly ages, whereas loss of *ter94* function significantly exacerbated this *Caz*-knockdown defect throughout the adult life span of these flies. We next examined the fly life span of the fly models with neuron-specific *Caz*-knockdown and genetically modified *ter94*. There were no significant differences in life spans among the control flies carrying *elav/+* (the average life span = 50.9 days, $n = 151$), neuron-specific *Caz*-knockdown flies carrying elav>UAS-*Caz*-IR (48.3 days, $n = 123$), and flies carrying the strongest loss-of-function allele of *ter94* and neuron-specific *Caz*-knockdown (elav> UAS-*Caz*-IR/*ter94*^{K15502}, 47.5 days, $n = 120$) (Supplementary Material, Fig. S3A). Similarly, there were no significant differences in life spans between neuron-specific *Caz*-knockdown flies carrying elav>UAS-*Caz*-IR/UAS-*GFP* (responder control, the average life span = 44.8 days, $n = 140$) and those carrying *ter94* overexpression in the background of neuron-specific *Caz*-knockdown, elav>UAS-*Caz*-IR/UAS-*ter94* (41.1 days, $n = 140$) (Supplementary Material, Fig. S3B). In our Caz-knockdown fly models, the expression of Caz protein was decreased to 40–60% in the CNS, but their life spans were not reduced (19). These results suggest that the substantial expression of Caz in neuronal tissues, even though it is not fully expressed, could sufficiently keep their life spans within normal range.

The effects of loss-of-function mutation and overexpression of *ter94* on the morphology of MN presynaptic terminals in the NMJs of neuron-specific *Caz*-knockdown flies

Based on the finding that our *Caz*-knockdown flies showed motor deficits in the climbing assay (19) and the fact that *FUS*, the human ortholog of *Caz*, is involved in ALS that impairs motor neurons, we analyzed the morphology of MN presynaptic

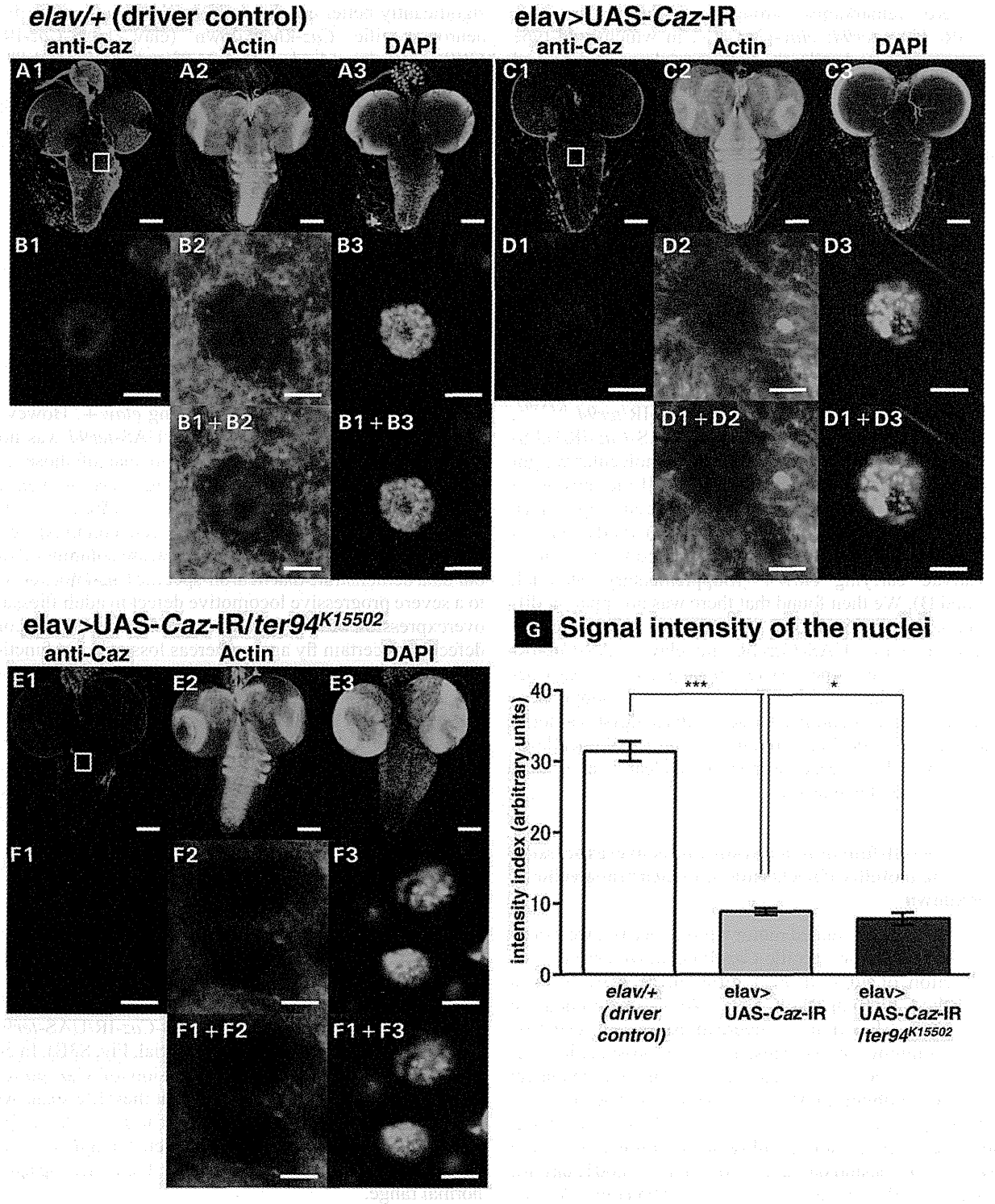

Figure 2. Neuron-specific *Caz*-knockdown reduces Caz signal in nuclei within larval CNS, and this reduction is significantly exacerbated by a loss-of-function *ter94* mutation. **(A)**–**(F)** are representative images of corresponding genotypes. (A1)–(A3) are immunofluorescent images of larval CNS, which comprises BVGC, taken from a driver control larva carrying *elav/+*. (C1)–(C3) are the BVGCs of a *Caz*-knockdown larva carrying UAS-*Caz*-IR. (E1)–(E3) are the BVGCs of a larva co-expressed with $ter94^{K15502}$ in the background of *Caz*-knockdown carrying elav>UAS-*Caz*-IR/$ter94^{K15502}$. (B1)–(B3), (D1)–(D3) and (F1)–(F3) are higher magnification images of the boxed area in (A1), (C1) and (E1), respectively. (B1+B2), (B1+B3), (D1+D2), (D1+D3), (F1+F2) and (F1+F3) are merged images. The indirect immunofluorescence in A1, B1, C1, D1, E1 and F1 is signal from the polyclonal anti-Caz antibody. The fluorescence in A2, B2, C2, D2, E2 and F2 is from phalloidin, which labels actin; the fluorescence in A3, B3, C3, D3, E3 and F3 is from DAPI, which labels DNA. The BVGC of driver control larvae carrying *elav/+* show ubiquitous signals from endogenous Caz (A1), but the signal intensity from endogenous Caz in the BVGC is remarkably reduced in larvae carrying elav>UAS-*Caz*-IR (C1). Anti-Caz antibody immunoreactivity is evident in the nuclei of neuronal cells (B1) and does not colocalize with phalloidin-stained actin filaments (B2, B1+B2). Caz does not colocalize with DAPI (B3, B1+B3). The intensity of nuclear Caz signal is significantly reduced in the BVGCs of larvae carrying

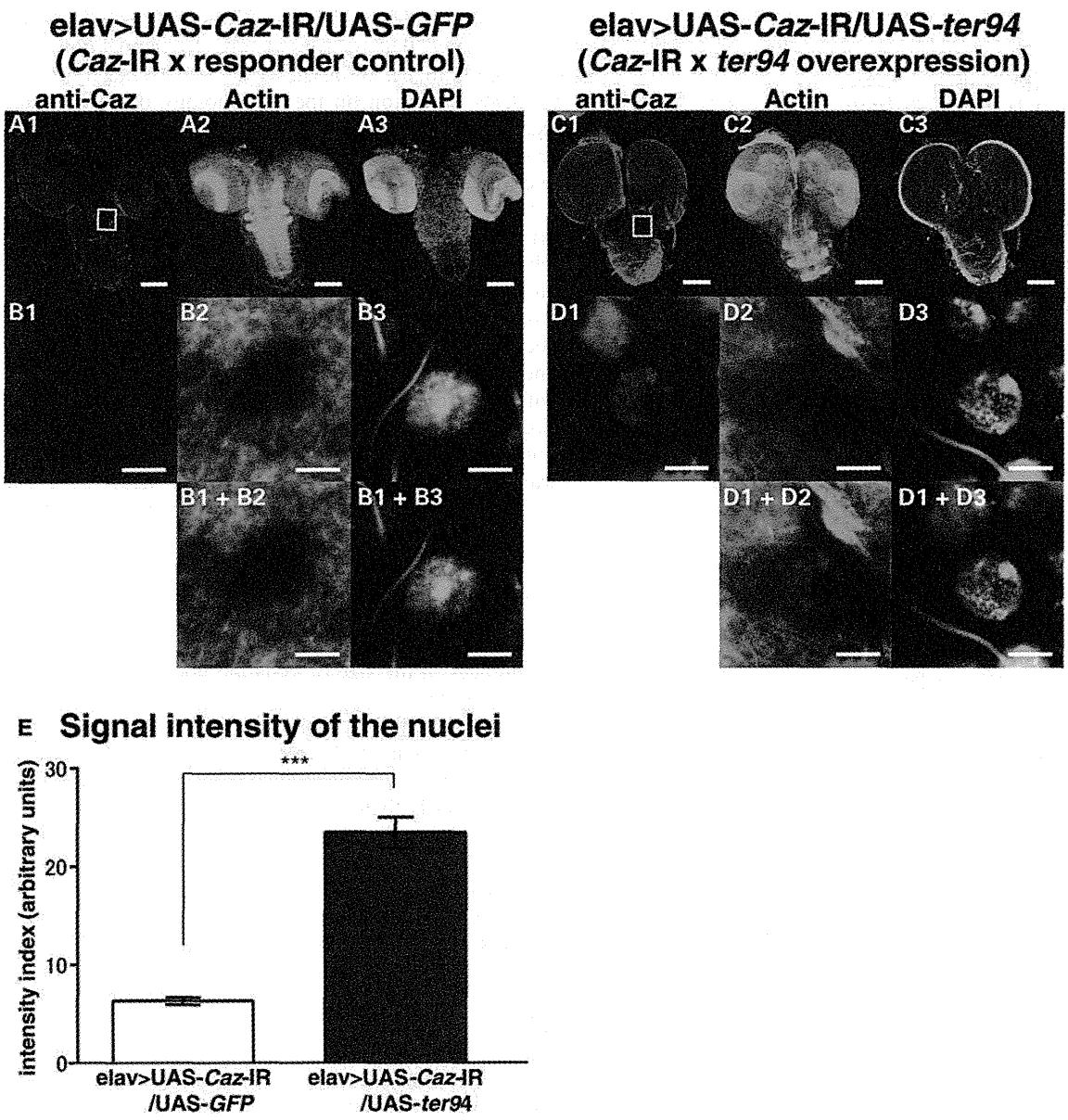

Figure 3. Overexpression of wild-type *ter94* restores Caz signal in nuclei in the CNS of larvae with neuron-specific *Caz*-knockdown. (**A**)–(**D**) are representative images of corresponding genotypes. (A1)–(A3) are the BVGCs of a *Caz*-knockdown larva carrying elav>UAS-*Caz*-IR/UAS-*GFP*. (C1)–(C3) are the BVGCs of a larva that overexpressed wild-type *ter94* in the background of *Caz*-knockdown carrying elav>UAS-*Caz*-IR/UAS-*ter94*. (B1)–(B3) and (D1)–(D3) are higher magnification images of the boxed area in A1 and C1, respectively. (B1+B2), (B1+B3), (D1+D2) and (D1+D3) are merged images. The indirect immunofluorescence in A1, B1, C1 and D1 is the signal from the polyclonal anti-Caz antibody. The fluorescence in A2, B2, C2 and D2 and that in A3, B3, C3 and D3 are from phalloidin and DAPI, respectively. (**E**) shows the mean (± SE) of the intensity of the nuclear Caz signal in the BVGC tissues from the third instar larvae as fluorescence emission in arbitrary units. Columns and horizontal bars show the mean and SE of 15 nuclei, respectively. $^{***}P < 0.001$. Compared with the Caz signals in the BVGCs of the larvae carrying elav>UAS-*Caz*-IR/UAS-*GFP* (A1), Caz signals are remarkably stronger in the BVGCs of the larvae carrying elav>UAS-*Caz*-IR/UAS-*ter94* (C1). The intensity of the nuclear Caz signal is significantly higher in these larvae due to the overexpression of *ter94* (D1) than in the larvae carrying elav>UAS-*Caz*-IR/UAS-*GFP* (B1) ($P < 0.001$, E). The scale bars indicate 100 μm (A1–A3 and C1–C3) and 5 μm (B1–B3 and D1–D3).

elav>UAS-*Caz*-IR (D1) compared with that of driver control larvae (B1) ($P < 0.001$, G). The larvae carrying the strongest loss-of-function allele of *ter94* and neuron-specific *Caz*-knockdown (elav>UAS-*Caz*-IR/*ter94*^{K15502}) (E1) also show remarkably reduced Caz signals in the BVGCs. The intensity of the nuclear Caz signal is significantly reduced in these larvae with the strongest loss-of-function allele of *ter94* and *Caz*-knockdown (F1), even compared with that of the *Caz*-knockdown larvae (D1) ($P < 0.05$, **G**). The scale bars indicate 100 μm (A1–A3, C1–C3 and E1–E3) and 5 μm (B1–B3, D1–D3 and F1–F3). (G) This graph plots the mean (± SE) of the intensity of the nuclear Caz signal in BVGCs from third instar larvae as fluorescence emission in arbitrary units with respect to the genotype; Columns and horizontal bars show the mean and SE of 15 nuclei, respectively. $^{***}P < 0.001$, $^{*}P < 0.05$.

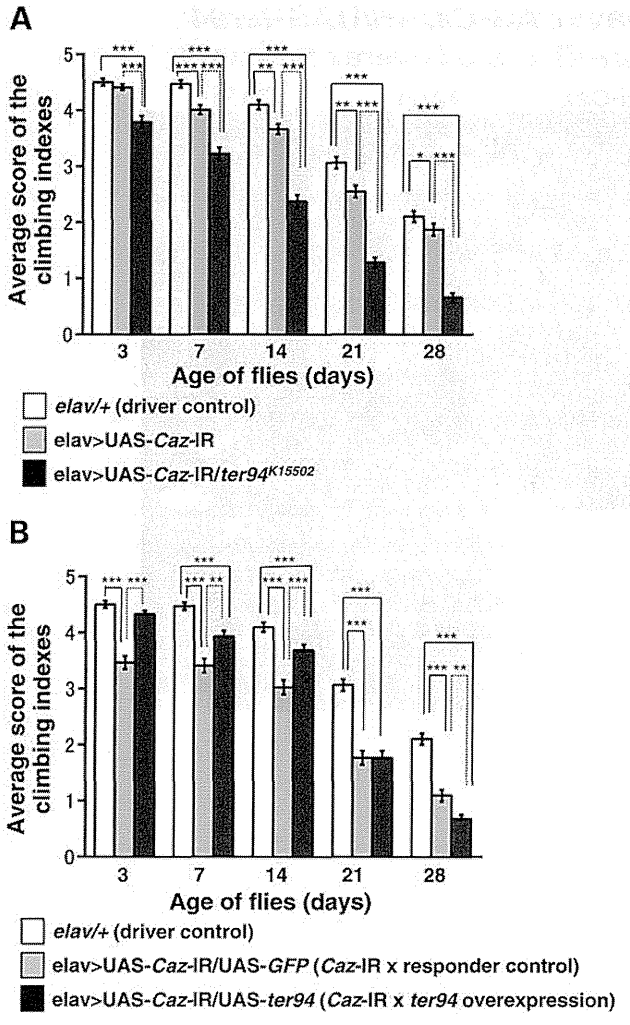

Figure 4. A loss-of-function *ter94* mutation and wild-type *ter94* overexpression have opposite effects on the climbing ability of neuron-specific *Caz*-knockdown flies. (**A**) The locomotive ability of driver control flies, which carrying *elav/+* ($n = 366$, white columns), is significantly better than that of neuron-specific *Caz*-knockdown flies, which carrying elav>UAS-*Caz*-IR ($n = 296$, gray columns) for every age examined other than day 3. On each day after eclosion that was monitored, adult flies carrying elav>UAS-*Caz*-IR/*ter94*^{K15502} ($n = 210$, black columns) exhibited significantly worse climbing ability than flies carrying neuron-specific *Caz*-knockdown alone. (**B**) Conversely, adult flies carrying elav>UAS-*Caz*-IR/UAS-*ter94* ($n = 215$, black columns) have significantly better climbing ability than flies carrying elav>UAS-*Caz*-IR/UAS-*GFP* ($n = 190$, gray columns) on days 3, 7 and 14, but not after day 14. The climbing ability of flies carrying *elav/+* ($n = 366$, white columns) is significantly better than those carrying elav>UAS-*Caz*-IR/UAS-*GFP* for every age examined, same as those in (A). Until day 3, the climbing ability of flies carrying elav>UAS-*Caz*-IR/UAS-*ter94* is recovered almost as well as that of flies carrying *elav/+*. However, that of the flies carrying elav>UAS-*Caz*-IR/UAS-*ter94* is significantly less than that of flies carrying *elav/+* after day 3. Columns and horizontal bars show the mean and SE of the measurements, respectively. $^{***}P < 0.001$, $^{**}P < 0.01$ and $^{*}P < 0.05$.

terminals at NMJs in *Caz*-knockdown flies. Abnormal NMJ morphology and behavioral defects have been implicated in many *Drosophila* models of neurodegenerative diseases that involve motor disturbances such as spinal muscular atrophy and tauopathies (30,31). Because most MNs of the adult fly originate from larval MNs, we examined the NMJ structure in the larvae from *Caz*-knockdown strains. Previously, we demonstrated that neuron-specific *Caz*-knockdown shortened terminal branches of larval MNs (19). To clarify the effects of the *ter94* mutation on the morphology of MN terminals, we examined the NMJ structure of our *Caz*-knockdown flies with or without *ter94* mutation and with or without wild-type *ter94* overexpression.

Compared with the total length of synaptic branches of MNs in driver control larvae carrying *elav/+* (94.4 ± 8.0 μm, Fig. 5A), which was significantly decreased in neuron-specific *Caz*-knockdown larvae carrying elav>UAS-*Caz*-IR (53.8 ± 6.0 μm, Fig. 5B; $P < 0.001$, Fig. 5D). Furthermore, this decreased branch length caused by neuron-specific *Caz*-knockdown was significantly enhanced by genetic crossing with the strongest loss-of-function allele of *ter94* (elav>UAS-*Caz*-IR/*ter94*^{K15502}, 39.5 ± 1.7 μm, Fig. 5C; $P = 0.035$, Fig. 5D). The average number of synaptic boutons per MN was also significantly smaller in neuron-specific *Caz*-knockdown larvae (9.7 ± 0.5, Fig. 5B) than in control larvae (14.7 ± 1.0, Fig. 5A; $P < 0.001$, Fig. 5E). This decrease in the number of synaptic boutons in the neuron-specific *Caz*-knockdown larvae was significantly enhanced by genetic crossing with the strongest loss-of-function allele of *ter94* (6.5 ± 0.5, Fig. 5C; $P < 0.001$, Fig. 5E). However, there were no significant differences in the size of synaptic boutons among these genotypes (Fig. 5F).

Conversely, the total branch length was significantly longer in the larvae with *ter94* overexpression in the background of neuron-specific *Caz*-knockdown (elav>UAS-*Caz*-IR/UAS-*ter94*, Fig. 5H and I) than in responder control larvae (elav>UAS-*Caz*-IR/UAS-*GFP*, Fig. 5G; 110.7 ± 12.0 versus 54.7 ± 2.5 μm, $P < 0.001$, Fig. 5J). The total branch length in the larvae carrying elav>UAS-*Caz*-IR/UAS-*GFP* was also significantly decreased compared with those carrying *elav/+* (94.4 ± 8.0 versus 54.7 ± 2.5 μm, $P < 0.001$, Fig. 5J). However, there were no significant differences about the total branch length between the larvae carrying *elav/+* and elav>UAS-*Caz*-IR/UAS-*ter94* (Fig. 5J). These results indicated that a loss-of-function *ter94* mutation and wild-type *ter94* overexpression have opposite effects on the synaptic terminal growth and morphogenesis that is impaired by *Caz*-knockdown. Notably, in the larvae with *ter94* overexpression in the background of neuron-specific *Caz*-knockdown (elav>UAS-*Caz*-IR/UAS-*ter94*), the extent of increase in the total branch length showed considerable variability (Fig. 5H and I). Of the larvae with *ter94* overexpression in the background of neuron-specific *Caz*-knockdown, 28% had branch lengths (Fig. 5I) that were 2-fold or more elongated relative to the responder controls (Fig. 5G). The larvae carrying elav>UAS-*Caz*-IR/UAS-*ter94* (Fig. 5H and I) also showed significantly increased number of synaptic boutons of MN terminals (25.6 ± 3.5) compared with those carrying elav>UAS-*Caz*-IR/UAS-*GFP* (8.7 ± 0.5, Fig. 5G; $P < 0.001$, Fig. 5K). The number of synaptic boutons in the larvae carrying elav>UAS-*Caz*-IR/UAS-*GFP* was also significantly decreased compared with that of those carrying *elav/+* (8.7 ± 0.5 versus 14.7 ± 1.0, $P < 0.01$, Fig. 5K). The number of synaptic boutons in the larvae carrying elav>UAS-*Caz*-IR/UAS-*ter94* was significantly increased compared with that of those carrying *elav/+* (14.7 ± 1.0 versus 25.6 ± 3.5, $P < 0.05$, Fig. 5K). The number of synaptic boutons of MNs might be increased in

the larvae carrying elav>UAS-*Caz*-IR/UAS-*ter94* due to the growth of synaptic terminals. There were no significant differences in the size of synaptic boutons among these genotypes (Fig. 5L). These results indicated that Caz is required for growth of MN terminals and formation of synaptic boutons at the NMJ, and these functions of Caz at the MN terminals are affected by the levels of ter94 protein.

DISCUSSION

Here, we demonstrated that eye-specific and neuron-specific *Caz*-knockdown induced a rough-eye phenotype and locomotive dysfunction, respectively; moreover, the locomotive dysfunction was due to the degeneration of MNs. The strongest loss-of-function allele of *ter94* (*ter94*^{k15502}) enhanced such rough-eye and locomotive-dysfunction phenotypes induced by *Caz*-knockdown. Conversely, the overexpression of wild-type *ter94* significantly suppressed the phenotypes induced by *Caz*-knockdown such as rough-eye phenotype, locomotive disabilities and degeneration of MNs. Moreover, neuron-specific *Caz*-knockdown decreased Caz levels in nuclei, and overexpression of wild-type *ter94* significantly suppressed the effects on nuclear *Caz*-expression levels induced by *Caz*-knockdown.

VCP is a member of the AAA protein family; these proteins are involved in diverse cellular functions and in a variety of physiological processes such as cell cycle regulation, membrane fusion, ER-associated degradation, ubiquitin-mediated protein degradation and nucleocytoplasmic shuttling (22–24). VCP is implicated in various neurodegenerative disorders. Mutations in the human *VCP* gene have been reported to cause frontotemporal dementia associated with IBMPFD or familial ALS, and VCP is consequently now considered as a causative gene for FTLD/ALS (25,26). Additionally, previous studies demonstrated that VCP is a binding partner of polyglutamine (polyQ) disease proteins with expanded polyQ tracts (huntingtin, ataxin-1, ataxin-3, ataxin-7 and androgen receptor) (32,33). Previously, the *Drosophila* ortholog of *VCP*, *ter94*, was identified in a screen for genetic modifiers of the eye degeneration phenotypes induced by eye-specific expression of an expanded polyQ tract (34). Moreover, VCP may be involved in diseases that are caused by changes in protein conformation; notably, VCP has been shown to colocalize with pathological protein aggregates in cases of Parkinson's disease, dementia with Lewy bodies, superoxide dismutase 1-associated ALS and Alzheimer's disease (32,35–37).

Our results demonstrate, for the first time, a genetic link between *Caz* and *ter94*, the *Drosophila* orthologs of *FUS* and *VCP*, respectively. Although it would be necessary to confirm whether that is *Drosophila*-specific or not, our results suggest genetic interaction between *FUS* and *VCP* in human. Genetic interaction between TDP-43 and VCP in *Drosophila* was demonstrated previously; IBMPFD-causing mutations in *ter94* lead to redistribution of TDP-43, from the nucleus to the cytoplasm, and redistribution of TDP-43 is sufficient to induce morphologically aberrant rough eyes (24). This previous report suggests that VCP can balance the amount of TDP-43, which is a constituent of larger heteronuclear ribonucleoprotein (hnRNP) complexes, between nucleus and cytoplasm by acting as a nucleocytoplasmic shuttling molecule (Fig. 6). In this schema, VCP functions to remove TDP-43 from RNP complexes, import TDP-43 into nuclei and degrade TDP-43 via autophagy (24,38,39). VCP might have similar functions with respect to FUS because FUS and TDP-43 have significant structural and functional similarities and are implicated in similar molecular processes (40–42). For example, TDP-43 and FUS act in the context of larger hnRNP complexes. FUS also continuously moves between the nucleus and the cytoplasm (16,17,43,44); therefore, FUS not only regulates gene expression in the nucleus, but also has important functions in the cytoplasm (5). Here, we showed that the decreased level of Caz in the nucleus and the resultant motor disturbance induced by neuron-specific *Caz*-knockdown could be rescued by overexpressed wild-type *ter94* despite lacking any change of Caz protein in the CNS (Supplementary Material, Fig. S1A and B). If VCP has a shuttling function as shown in Figure 6, wild-type ter94 overexpression could translocate Caz from cytoplasm to nucleus because nuclear importing function of ter94 would be dominantly induced in the situation with the deficiency of Caz in the nucleus. Conversely, the loss-of-function allele of *ter94* (*ter94*^{k15502}) exacerbated the depletion of *Caz* from the nucleus probably because ter94-mediated nuclear import of Caz was compromised.

It has been demonstrated that a polyQ tract can interact with VCP in *Drosophila* (34); specifically, either the strongest (*ter94*^{k15502}) or strong (*ter94*^{03775}) loss-of-function allele of *ter94* suppressed the eye degeneration induced by an expanded polyQ tract, whereas the overexpression of wild-type *ter94* in the background of *Caz*-knockdown enhanced this phenotype. Additionally, a chromosomal deletion of 46C3–46E02, the genomic region that contains *ter94*, acted as a dominant suppressor of the polyQ-induced phenotype (34). Our present study and these previous reports together indicate that gain and loss of *ter94* function rescued and exacerbated *Caz*-knockdown phenotypes, respectively, and that they had the converse effects on polyQ-induced phenotypes. These converse effects could be explained by the difference in disease pathogenesis; in polyQ-induced disease models, polyQ-containing pathogenic aggregates exist in nuclei of affected neurons; in contrast, Caz expression in nuclei is deficient in *Caz*-knockdown disease models. Overexpression of wild-type *ter94*, which functions in nuclear import of polyQ or Caz, would exacerbate nuclear polyQ aggregation, but could alleviate the nuclear deficiency of Caz protein.

Neuron-specific *Caz*-knockdown flies showed an age-dependent decline in climbing ability that was significantly worse than driver control flies for every age examined after day 7. Overexpression of wild-type *ter94* significantly rescued the declined locomotor ability caused by *Caz*-knockdown up to day 14, but it did not rescue the phenotype at later stages. Regarding the age-dependent ability to rescue locomotive deficits, we considered the two following possible explanations. First, the elongation of the branch length of MN terminals at NMJs caused by overexpression of wild-type *ter94* in neuron-specific *Caz*-knockdown flies may have alleviated the locomotive defects caused by neuron-specific *Caz*-knockdown. However, the extent of this elongation was highly variable. A previous report showed that larvae with NMJ overgrowth phenotypes exhibited mobility defects; this finding indicates that the elongation of nerve terminal branches beyond some adequate

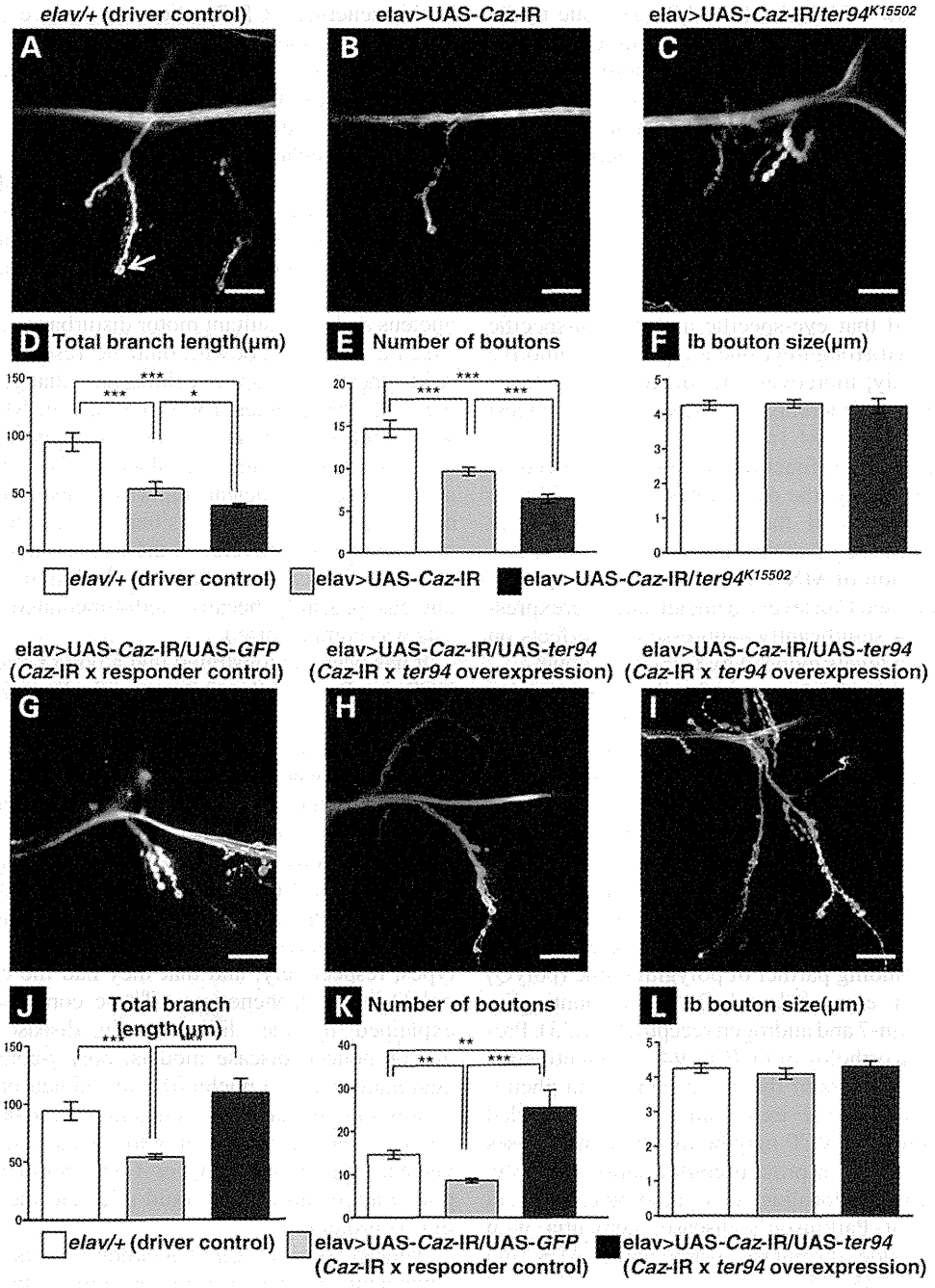

Figure 5. A loss-of-function *ter94* mutation and wild-type *ter94* overexpression change the morphology of MN presynaptic terminals in the NMJ of MN4 in neuron-specific *Caz*-knockdown larvae in opposite ways. A representative image of anti-horseradish peroxidase staining of muscle 4 synapses in third instar larvae with *elav/+* (**A**; a driver control), neuron-specific *Caz*-knockdown (**B**; elav>UAS-*Caz*-IR), neuron-specific *Caz*-knockdown crossed with the strongest loss-of-function mutation of *ter94* (**C**; elav>UAS-*Caz*-IR/*ter94*^{K15502}), neuron-specific *Caz*-knockdown crossed with UAS-*GFP* (**G**; elav>UAS-*Caz*-IR/UAS-*GFP*; a responder control) or neuron-specific *Caz*-knockdown crossed with UAS-*ter94* (**H** and **I**; different larvae with the same genotype, elav>UAS-*Caz*-IR/UAS-*ter94*). (**D** and **J**) Total branch length of the NMJ from muscle 4 for each of the indicated genotypes. Compared with the total length of synaptic branches of MNs in driver control larvae (A), that in neuron-specific *Caz*-knockdown larvae (B) is significantly decreased ($P < 0.001$, $n = 10$, D). This decrease in branch length observed in the neuron-specific *Caz*-knockdown larvae (B) is significantly worsened in larvae carrying the strongest loss-of-function allele of *ter94* and neuron-specific *Caz*-knockdown (C) ($P < 0.05$, $n = 10$, D). Conversely, the total branch length in larvae that overexpressed wild-type *ter94* in the background of neuron-specific *Caz*-knockdown (H and I) is significantly longer than that in larvae carrying elav>UAS-*Caz*-IR/UAS-*GFP* (G) ($P < 0.001$, $n = 14$, J). The extent of increase in the total branch length of elav>UAS-*Caz*-IR/UAS-*ter94* was highly variable among individual flies (H and I). The total branch length of synaptic branches of MNs in the larvae carrying elav>UAS-*Caz*-IR/UAS-*GFP* is significantly decreased compared with that of larvae carrying *elav/+* ($P < 0.001$, $n = 12$, J). (**E** and **K**) The number of synaptic boutons for each of the indicated genotypes. The number of synaptic boutons of MNs in neuron-specific *Caz*-knockdown larvae (B) is also significantly decreased compared with driver control larvae (A) ($P < 0.001$, $n = 10$, E). This decrease in the number of synaptic boutons in the neuron-specific *Caz*-knockdown larvae is significantly worsened in larvae carrying the strongest loss-of-function allele of *ter94* and neuron-specific *Caz*-knockdown (C) ($P < 0.001$, $n = 10$, E). Conversely, the number of synaptic boutons in the larvae carrying wild-type *ter94* overexpression in the background of neuron-specific *Caz*-knockdown (H and I) is significantly higher than that in responder control larvae (G) ($P < 0.001$, $n = 10$, K). Compared with the larvae carrying *elav/+*, the number of synaptic

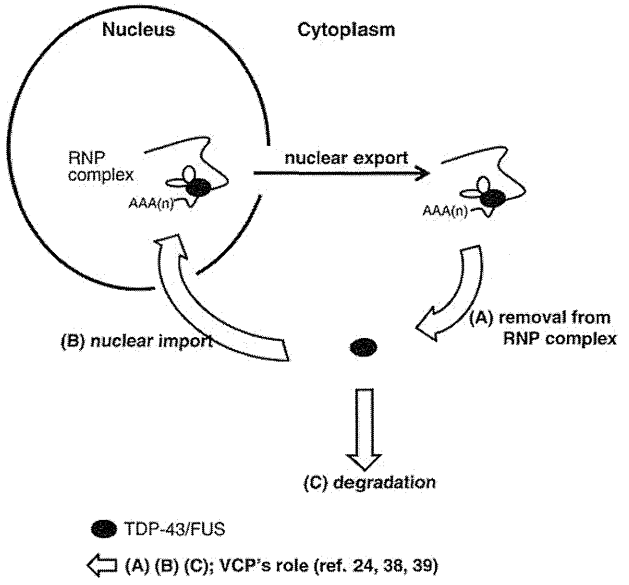

Figure 6. Hypothetical roles of VCP in the nucleoplasmic balance of TDP-43 and FUS referring to the paper by Ritson *et al.* (24). VCP, human ortholog of ter94, may act during removal of TDP-43/FUS from RNP complexes in the cytoplasm (**A**), nuclear import of TDP-43/FUS (**B**) and degradation of TDP-43/FUS by the autophagic pathway (**C**). FUS, the human ortholog of Caz, might translocate from cytoplasm to nucleus when VCP is overexpressed because the nuclear-import function of VCP (B) would be dominantly induced under conditions of FUS deficiency in nuclei. Conversely, loss-of-function alleles of VCP may exacerbate the FUS deficiency in nuclei because FUS is not being properly imported into nuclei by VCP.

length could cause disturbances in locomotive ability (45). Therefore, synaptic MN terminals may have to be within some optimal range of lengths. Second, the age-dependence of ability to rescue the locomotive defects might be due to the age-dependent difference in the expression levels of ter94. Tissue expression data from FlyBase (http://flybase.org) show that mRNA expression levels of *ter94* are very high in the CNS of third instar larvae, but they are relatively low in the head, eye or brain of adults. Age-dependent changes in ter94 expression levels might determine the period within which wild-type ter94 overexpression can rescue locomotive deficits caused by *Caz*-knockdown. Age-dependent effects of ter94 are also evident in fly models of polyQ-induced neurodegeneration. Between the third instar larval stage and the late pupal stage, levels of ter94 were elevated, and elevated levels of ter94 induced severe apoptotic cell death in those pupae (34).

In some IBMPFD-associated VCP mutants, it was previously reported that pathogenic VCPs could bind to cofactors, such as Npl4, Ufd1 or p47, more efficiently than wild-type VCP (46,47). However, little is known about which of the VCP cofactors relate to FUS-nuclear translocation or how the conformational change of VCP affects the interactions of VCP cofactors with other proteins.

In conclusion, we found a genetic interaction between *Caz* and *ter94*. Our data indicate that chemicals that up-regulate the function of VCP or facilitate nuclear import of FUS may suppress the pathogenic processes that lead to the degeneration of MNs in FUS-associated ALS/FTLD. This might be the first step to develop candidate drugs for the disease-modifying therapy of human ALS.

MATERIALS AND METHODS

Fly stocks

Fly stocks were maintained at 25°C on standard food containing 0.7% agar, 5% glucose and 7% dry yeast. Canton S was used as the wild-type strain. The strain: w^{1118}; *P {w [+mC] = UAS-GFP. nls} 14* (DGRC number 107870) (UAS-*GFP*) and chromosomal deficiency line: *Df (2R) X1*, $Mef2^{X1}$/*CyO*, Adh^{nB} (DGRC number 106718) were obtained from the Kyoto *Drosophila* Genetic Resource Center. The strains: *w* [*]; *P {[+mC] = GAL4-elav.L} 3* (Bloomington BL8760) (*elav-GAL4*), $y^1 w$ [*]; *P {[+mC] = Act5C-GAL4} 17bFO1/TM6B*, Tb^1 (BL3954) (*Act5C-GAL4*), $y^1 w^{67c23}$; *P {w [+mC] = lacW}* $ter94^{K15502}$/*CyO* (BL10454) ($ter94^{K15502}$) and $cn^1 P$ {*ry* [+*t7.2*] = *PZ*} $ter94^{03775}$/*CyO*; ry^{506} (BL11349) ($ter94^{03775}$) were obtained from the Bloomington *Drosophila* stock center in Indiana. Establishment of the lines carrying *GMR-GAL4* was as described previously (48). We crossed transgenic UAS-*Caz*-IR flies with *Act5C-GAL4*, *GMR-GAL4* or *elav-GAL4* flies to drive expression of *Caz* dsRNA throughout the whole body of flies, specifically in eye imaginal discs or specifically in neuronal tissues, respectively. We generated eye-specific *Caz*-knockdown flies (*GMR-GAL4*; UAS-*Caz*-IR/+; +) (GMR>UAS-*Caz*-IR) and neuron-specific Caz-knockdown flies (w; UAS-*Caz*-IR/+; *elav-GAL4*/+) (elav>UAS-*Caz*-IR). Each transgenic strain showed a consistent phenotype (Table 1).

Dr Kakizuka kindly provided UAS-*ter94* flies. The UAS-*ter94*-IR strain: w^{1118}; *P {GD9777} v24354* (VDRC number v24354) (*ter94*-knockdown) was obtained from the VDRC. VDRC reports that the *ter94*-RNAi construct is inserted into chromosome 2 and has no off-target effects. The lines generated in this study are as follows: *GMR-GAL4*; +; + (*GMR*), *GMR-GAL4*; UAS-*Caz*-IR363−399/+; + (GMR>UAS-*Caz*-IR), *GMR-GAL4*; UAS-*Caz*-IR363−399/UAS-*Caz*-IR363−399; + (GMR>UAS-*Caz*-IR/UAS-*Caz*-IR), *GMR-GAL4*; UAS-*Caz*-IR363−399/$ter94^{K15502}$; + (GMR>UAS-*Caz*-IR/$ter94^{K15502}$), *GMR-GAL4*; UAS-*Caz*-IR363−399/$ter94^{03775}$; + (GMR>UAS-*Caz*-IR/$ter94^{03775}$), *GMR-GAL4*; UAS-*Caz*-IR363−399/UAS-*GFP*; + (GMR>UAS-*Caz*-IR/UAS-*GFP*), *GMR-GAL4*; UAS-*Caz*-IR363−399/UAS-*ter94*; + (GMR>UAS-*Caz*-IR/UAS-*ter94*), w; +; *elav-GAL4*/+ (*elav*/+; a driver control), UAS-*Caz*-IR363−399/+ (UAS-*Caz*-IR/+; a responder control), $ter94^{K15502}$/+, w; UAS-*Caz*-IR363−399/+; *elav-GAL4*/+ (elav> UAS-*Caz*-IR), w; UAS-*Caz*-IR363−399/UAS-*Caz*-IR363−399;

boutons is significantly decreased in the larvae carrying elav>UAS-*Caz*-IR/UAS-*GFP* ($P < 0.001$, $n = 10$, K), but significantly increased in those carrying elav> UAS-*Caz*-IR/UAS-*ter94* ($P < 0.05$, $n = 14$, K). (**F** and **L**) The size of synaptic boutons for each of the indicated genotypes. The size of Ib bouton (indicated with an arrow in A) was measured ($n = 31$ for *elav*/+, $n = 33$ for elav>UAS-*Caz*-IR, $n = 31$ for elav>UAS-*Caz*-IR/$ter94^{K15502}$, $n = 30$ for elav>UAS-*Caz*-IR/UAS-*GFP* and $n = 32$ for elav>UAS-*Caz*-IR/UAS-*ter94*). There are no significant differences in the size of synaptic boutons among driver control larvae, either larvae with elav>UAS-*Caz*-IR and those with elav>UAS-*Caz*-IR/$ter94^{K15502}$ (F) or among driver control larvae, either larvae with elav>UAS-*Caz*-IR/UAS-*GFP* and elav>

elav-GAL4/elav-GAL4 (elav>UAS-*Caz*-IR/UAS-*Caz*-IR), w; UAS-*Caz*-IR363−399/*ter94*^{K15502}; *elav-GAL4/+* (elav> UAS-*Caz*-IR/*ter94*^{K15502}), w; UAS-*Caz*-IR363−399/ UAS-*GFP*; *elav-GAL4/+* (elav>UAS-*Caz*-IR/UAS-*GFP*), w; UAS-*Caz*-IR363−399/UAS-*ter94*; *elav-GAL4/+* (elav>UAS-*Caz*-IR/ UAS-*ter94*).

Immunohistochemistry

Rabbit anti-Caz antibodies were raised against amino acid residues 29−45 and 383−399 of Caz and were produced previously (19). For immunohistochemical analysis, CNS tissues were dissected from third instar larvae and fixed in 4% paraformaldehyde/phosphate buffered saline (PBS) for 15 min at 25°C. These tissue samples were washed with PBS containing 0.3% Triton X-100; fixed samples were then incubated with Alexa 488-conjugated phalloidin (1 unit/200 μl) in PBS containing 0.3% Triton X-100 for 20 min at 25°C. The samples were then blocked with blocking buffer (PBS containing 0.15% Triton X-100 and 10% normal goat serum) for 30 min at 25°C, and then incubated with 1 : 1000 diluted rabbit anti-Caz antibody in the blocking buffer for 20 h at 4°C. After extensive washing with PBS containing 0.3% Triton X-100, samples were incubated in the dark with secondary antibodies labeled with Alexa 546 (1 : 400; Invitrogen) diluted in the blocking buffer for 3 h at 25°C. After washing with PBS containing 0.3% Triton X-100, the samples were stained with DAPI (0.5 μg/ml)/PBS/ 0.1% Triton X-100. After extensive washing with PBS containing 0.1% Triton X-100 and PBS, the samples were mounted in Vectashield (Vector Laboratories-Inc.) and observed under a confocal laser scanning microscope (OLYMPUS FLUOVIEW FV10i). Images were analyzed with the program MetaMorph Imaging System 7.7 (Molecular Devices Inc.). The use of this program made it possible to quantify the average and the standard error of fluorescence emission from nuclei of each fly strain.

For NMJ staining, third instar larvae were dissected in HL3 saline (49), and then fixed in 4% paraformaldehyde/PBS for 30 min. The blocking buffer contained 2% bovine serum albumin and 0.1% Triton X-100 in PBS. Fluorescein isothiocyanate-conjugated goat anti-horseradish peroxidase (HRP) (1:1000, MP Biochemicals) was used as the detection antibody. The samples were mounted and observed under a confocal laser scanning microscope (Carl Zeiss LSM510, Jena, Germany). MN 4 (Ib) in muscle 4 in abdominal segment 2 was quantified. Images were acquired using a Zeiss LSM 510 confocal laser scanning microscope by merging 1 μm interval z-sections onto a single plane. The MetaMorph imaging system was used to measure nerve terminal branch lengths and Ib bouton sizes.

Immunoblotting analysis

Protein extracts from the CNS of *Drosophila* carrying *elav/+*, elav>UAS-*Caz*-IR, elav>UAS-*Caz*-IR/*ter94* ^{K15502}, elav> UAS-*Caz*-IR/UAS-*GFP* and elav>UAS-*Caz*-IR/UAS-*ter94* larvae were prepared as described previously (19). Briefly, the CNS was excised from third instar larvae and homogenized in a sample buffer containing 50 mM Tris–HCl (pH 6.8), 2% sodium dodecyl sulfate (SDS), 10% glycerol, 0.1% bromophenol blue and 1.2% β-mercaptoethanol. The homogenates were boiled at 100°C for 5 min and then centrifuged. The supernatants (extracts) were electrophoretically separated on SDS-polyacrylamide gels containing 12% acrylamide and then transferred to polyvinylidene difluoride membranes (Merck, Millipore, MA, USA). The blotted membranes were blocked with tris-buffered saline/ 0.05% Tween containing 5% skim milk for 1 h at 25°C, followed by incubation with rabbit polyclonal anti-Caz at a 1:5000 dilution for 16 h at 4°C. After washing, the membranes were incubated with HRP-conjugated anti-rabbit IgG (Thermo Scientific, IL, USA) at 1:10 000 dilution for 2 h at 25°C. Antibody binding was detected using ECL Western blotting detection reagents (Thermo Scientific) and images were analyzed using an ImageQuant^{TM} LAS 4000 image analyzer (GE Healthcare Bioscience, Tokyo, Japan). To compare Caz protein levels in the CNS extracts of those larvae, densitometric quantification of the 45-kDa Caz protein bands was carried out. The relative band intensities were quantified and normalized to Coomassie Brilliant Blue staining, then expressed as the percentage of the band intensity derived from larvae carrying *elav/+*.

Scanning electron microscopy

Adult flies were anesthetized with 99% diethyl ether, mounted on stages and observed under an SEM V-7800 (Keyence Inc.) in the low vacuum mode (50). In every experiment, at least five adult flies were chosen from each line for scanning electron microscopy to assess the eye phenotype. For each experiment, there was no significant variation in eye phenotype among the five individuals from the same strain.

Longevity assay

Longevity assays were carried out in a humidified, temperature-controlled incubator set at 25°C and 60% humidity on a 12-h light and 12-h dark cycle; flies were maintained on standard fly food. Flies carrying *elav/+* ($n = 151$), elav>UAS-*Caz*-IR ($n = 123$), elav>UAS-*Caz*-IR/*ter94*^{K15502} ($n = 120$), elav> UAS-*Caz*-IR/UAS-*GFP* ($n = 140$) or elav>UAS-*Caz*-IR/ UAS-*ter94* ($n = 140$) were placed at 28°C, and newly eclosed adult male flies were separated and placed in vials at a low density (20 flies per vial). Every 3 days, they were transferred to new tubes containing fresh food and deaths were scored. The survival rate was determined by plotting a graph of the percentage of surviving flies among total flies at the starting point of each experiment versus days.

Climbing assay

Climbing assays were performed as described previously (29). Flies carrying *elav/+*, UAS-*Caz*-IR/+, *ter94*^{K15502}/+, elav> UAS-*Caz*-IR, elav>UAS-*Caz*-IR/*ter94*^{K15502}, elav>UAS-*Caz*-IR/UAS-*GFP* and elav>UAS-*Caz*-IR/UAS-*ter94* were placed at 28°C, and newly eclosed adult male flies were separated and placed in vials at a density of 20 flies per vial. Flies were transferred, without anesthesia, to a conical tube. The tubes were tapped to collect the flies to the bottom, and they were then given 30 s to climb the wall. After 30 s, the flies were collected at the bottom by tapping of the tube and were again allowed to climb for 30 s. Similar procedures, all of which were videotaped, were repeated five times in total. For each climbing experiment, the height to which each fly

climbed was scored as score (height climbed); 0 (less than 2 cm), 1 (between 2 and 3.9 cm), 2 (between 4 and 5.9 cm), 3 (between 6 and 7.9 cm), 4 (between 8 and 9.9 cm) or 5 (greater than 10 cm). The climbing index for each fly strain was calculated as follows; each score was multiplied by the number of flies for which that score was recorded, and the products were summed up, then divided by five times the total number of flies examined. These climbing assays were carried out every 7 days until the 28th day after eclosion.

Data analysis

GraphPad Prism version 6.0 was used to perform each statistical analysis. The Mann–Whiney test was used for the assessment of the statistical significance of comparisons between two groups of data. For other assays, one-way analysis of variance (ANOVA) was used to determine the statistical significance of comparisons between groups of data. When the two-way ANOVA showed significant variation among groups, a subsequent Dunnett's test was used for pairwise comparisons between groups. All data are shown as mean ± standard error (SE).

SUPPLEMENTARY MATERIAL

Supplementary Material is available at *HMG* online.

ACKNOWLEDGEMENTS

We would like to thank Dr Kakizuka for generously providing us the UAS-*ter94* fly strains used in these experiments. We would also like to acknowledge Dr H. Yoshida, Ms R. Sahashi, Mr K. Morishita and Mr K. Shimaji for valuable discussion, technical support and suggestions. We thank the Bloomington *Drosophila* stock center, the Vienna *Drosophila* RNAi center and Kyoto *Drosophila* Genetic Resource Center for giving us fly lines.

Conflict of Interest statement. None declared.

FUNDING

This work was supported by Grants-in-Aid from the Research Committee of CNS. Degenerative Diseases, the Ministry of Health, Labour and Welfare of Japan (T.T.), and partly supported by "Integrated Research on Neuropsychiatric Disorders" carried out under the Strategic Research Program for Brain Sciences by the Ministry of Education, Culture, Sports, Science and Technology of Japan (Y.N.). The funders had no role in study design, data collection and analysis, decision to publish or preparation of the manuscript.

REFERENCES

1. Boillée, S., Vande Velde, C. and Cleveland, D.W. (2006) ALS: a disease of motor neurons and their nonneuronal neighbors. *Neuron*, **52**, 39–59.
2. Mackenzie, I.R., Rademakers, R. and Neumann, M. (2010) TDP-43 and FUS in amyotrophic lateral sclerosis and frontotemporal dementia. *Lancet Neurol.*, **9**, 995–1007.
3. Lomen-Hoerth, C., Anderson, T. and Miller, B. (2002) The overlap of amyotrophic lateral sclerosis and frontotemporal dementia. *Neurology*, **59**, 1077–1079.
4. Murphy, J.M., Henry, R.G., Langmore, S., Kramer, J.H., Miller, B.L. and Lomen-Hoerth, C. (2007) Continuum of frontal lobe impairment in amyotrophic lateral sclerosis. *Arch. Neurol.*, **64**, 530–534.
5. Dormann, D. and Haass, C. (2013) Fused in sarcoma (FUS): an oncogene goes awry in neurodegeneration. *Mol. Cell Neurosci.*, **56**, 475–486.
6. Lemmens, R., Moore, M.J., Al-Chalabi, A., Brown, R.H. Jr. and Robberecht, W. (2010) RNA metabolism and the pathogenesis of motor neuron diseases. *Trends Neurosci.*, **33**, 249–258.
7. Gitcho, M.A., Baloh, R.H., Chakraverty, S., Mayo, K., Norton, J.B., Levitch, D., Hatanpaa, K.J., White, C.L. 3rd., Bigio, E.H., Caselli, R. *et al.* (2008) TDP-43 A315 T mutation in familial motor neuron disease. *Ann. Neurol.*, **63**, 535–538.
8. Yokoseki, A., Shiga, A., Tan, C.F., Tagawa, A., Kaneko, H., Koyama, A., Eguchi, H., Tsujino, A., Ikeuchi, T., Kakita, A. *et al.* (2008) TDP-43 mutation in familial amyotrophic lateral sclerosis. *Ann. Neurol.*, **63**, 538–542.
9. Kabashi, E., Valdmanis, P.N., Dion, P., Spiegelman, D., McConkey, B.J., Vande Velde, C., Bouchard, J.P., Lacomblez, L., Pochigaeva, K., Salachas, F. *et al.* (2008) TARDBP mutations in individuals with sporadic and familial amyotrophic lateral sclerosis. *Nat. Genet.*, **40**, 572–574.
10. Sreedharan, J., Blair, I.P., Tripathi, V.B., Hu, X., Vance, C., Rogelj, B., Ackerley, S., Durnall, J.C., Williams, K.L., Buratti, E. *et al.* (2008) TDP-43 mutations in familial and sporadic amyotrophic lateral sclerosis. *Science*, **319**, 1668–1672.
11. Pesiridis, G.S., Lee, V.M. and Trojanowski, J.Q. (2009) Mutations in TDP-43 link glycine-rich domain functions to amyotrophic lateral sclerosis. *Hum. Mol. Genet.*, **18**, R156–R162.
12. Kwiatkowski, T.J. Jr., Bosco, D.A., Leclerc, A.L., Tamrazian, E., Vanderburg, C.R., Russ, C., Davis, A., Gilchrist, J., Kasarskis, E.J., Munsat, T. *et al.* (2009) Mutations in the FUS/TLS gene on chromosome 16 cause familial amyotrophic lateral sclerosis. *Science*, **323**, 1205–1208.
13. Vance, C., Rogelj, B., Hortobágyi, T., De, Vos, K.J., Nishimura, A.L., Sreedharan, J., Hu, X., Smith, B., Ruddy, D., Wright, P. *et al.* (2009) Mutations in FUS, an RNA processing protein, cause familial amyotrophic lateral sclerosis type 6. *Science*, **323**, 1208–1211.
14. Hewitt, C., Kirby, J., Highley, J.R., Hartley, J.A., Hibberd, R., Hollinger, H.C., Williams, T.L., Ince, P.G., McDermott, C.J. and Shaw, P.J. (2010) Novel FUS/TLS mutations and pathology in familial and sporadic amyotrophic lateral sclerosis. *Arch. Neurol.*, **67**, 455–461.
15. Rademakers, R., Stewart, H., Dejesus-Hernandez, M., Krieger, C., Graff-Radford, N., Fabros, M., Briemberg, H., Cashman, N., Eisen, A. and Mackenzie, I.R. (2010) Fus gene mutations in familial and sporadic amyotrophic lateral sclerosis. *Muscle Nerve*, **42**, 170–176.
16. Zinszner, H., Sok, J., Immanuel, D., Yin, Y. and Ron, D. (1997) TLS (FUS) binds RNA in vivo and engages in nucleo-cytoplasmic shuttling. *J. Cell Sci.*, **110**, 1741–1750.
17. Lagier-Tourenne, C., Polymenidou, M. and Cleveland, D.W. (2010) TDP-43 and FUS/TLS: emerging roles in RNA processing and neurodegeneration. *Hum. Mol. Genet.*, **19**, R46–R64.
18. Feiguin, F., Godena, V.K., Romano, G., D'Ambrogio, A., Klima, R. and Baralle, F.E. (2009) Depletion of TDP-43 affects *Drosophila* motoneurons terminal synapsis and locomotive behavior. *FEBS Lett.*, **583**, 1586–1592.
19. Sasayama, H., Shimamura, M., Tokuda, T., Azuma, Y., Yoshida, T., Mizuno, T., Nakagawa, M., Fujikake, N., Nagai, Y. and Yamaguchi, M. (2012) Knockdown of the *Drosophila* fused in sarcoma (FUS) homologue causes deficient locomotive behavior and shortening of motoneuron terminal branches. *PLoS One*, **7**, e39483.
20. Kabashi, E., Bercier, V., Lissouba, A., Liao, M., Brustein, E., Rouleau, G.A. and Drapeau, P. (2011) FUS and TARDBP but not SOD1 interact in genetic models of amyotrophic lateral sclerosis. *PLoS Genet.*, **7**, e1002214.
21. Wang, J.W., Brent, J.R., Tomlinson, A., Shneider, N.A. and McCabe, B.D. (2011) The ALS-associated proteins FUS and TDP-43 function together to affect *Drosophila* locomotion and life span. *J. Clin. Invest.*, **121**, 4118–4126.
22. Meyer, H., Bug, M. and Bremer, S. (2012) Emerging functions of the VCP/p97 AAA-ATPase in the ubiquitin system. *Nat. Cell Biol.*, **14**, 117–123.
23. Braun, R.J. and Zischka, H. (2008) Mechanisms of Cdc48/VCP-mediated cell death: from yeast apoptosis to human disease. *Biochim. Biophys. Acta*, **1783**, 1418–1435.

24. Ritson, G.P., Custer, S.K., Freibaum, B.D., Guinto, J.B., Geffel, D., Moore, J., Tang, W., Winton, M.J., Neumann, M., Trojanowski, J.Q. *et al.* (2010) TDP-43 mediates degeneration in a novel *Drosophila* model of disease caused by mutations in VCP/p97. *J. Neurosci.*, **30**, 7729–7739.
25. Watts, G.D., Wymer, J., Kovach, M.J., Mehta, S.G., Mumm, S., Darvish, D., Pestronk, A., Whyte, M.P. and Kimonis, V.E. (2004) Inclusion body myopathy associated with Paget disease of bone and frontotemporal dementia is caused by mutant valosin-containing protein. *Nat. Genet.*, **36**, 377–381.
26. Johnson, J.O., Mandrioli, J., Benatar, M., Abramzon, Y., Van, Deerlin, V.M., Trojanowski, J.Q., Gibbs, J.R., Brunetti, M., Gronka, S., Wuu, J. *et al.* (2010) Exome sequencing reveals VCP mutations as a cause of familial ALS. *Neuron*, **68**, 857–864.
27. Stolow, D.T. and Haynes, S.R. (1995) Cabeza, a *Drosophila* gene encoding a novel RNA binding protein, shares homology with EWS and TLS, two genes involved in human sarcoma formation. *Nucleic Acids Res.*, **23**, 835–843.
28. Ruden, D.M., Sollars, V., Wang, X., Mori, D., Alterman, M. and Lu, X. (2000) Membrane fusion proteins are required for oskar mRNA localization in the *Drosophila* egg chamber. *Dev. Biol.*, **218**, 314–325.
29. Shcherbata, H.R., Yatsenko, A.S., Patterson, L., Sood, V.D., Nudel, U., Yaffe, D., Baker, D. and Ruohola-Baker, H. (2007) Dissecting muscle and neuronal disorders in a *Drosophila* model of muscular dystrophy. *EMBO J.*, **26**, 481–493.
30. Chang, H.C., Dimlich, D.N., Yokokura, T., Mukherjee, A., Kankel, M.W., Sen, A., Sridhar, V., Fulga, T.A., Hart, A.C., Van Vactor, D. *et al.* (2008) Modeling spinal muscular atrophy in *Drosophila*. *PLoS One*, **3**, e3209.
31. Chee, F., Mudher, A., Newman, T.A., Cuttle, M., Lovestone, S. and Shepherd, D. (2006) Overexpression of tau results in defective synaptic transmission in *Drosophila* neuromuscular junctions. Biochem. Soc. Trans., **34**, 88–90.
32. Hirabayashi, M., Inoue, K., Tanaka, K., Nakadate, K., Ohsawa, Y., Kamei, Y., Popiel, A.H., Sinohara, A., Iwamatsu, A., Kimura, Y. *et al.* (2001) VCP/p97 in abnormal protein aggregates, cytoplasmic vacuoles, and cell death, phenotypes relevant to neurodegeneration. *Cell Death Differ.*, **8**, 977–984.
33. Fujita, K., Nakamura, Y., Oka, T., Ito, H., Tamura, T., Tagawa, K., Sasabe, T., Katsuta, A., Motoki, K., Shiwaku, H. *et al.* (2013) A functional deficiency of TERA/VCP/p97 contributes to impaired DNA repair in multiple polyglutamine diseases. *Nat. Commun.*, **4**, 1816. doi:10.1038/ncomms2828.
34. Higashiyama, H., Hirose, F., Yamaguchi, M., Inoue, Y.H., Fujikake, N., Matsukage, A. and Kakizuka, A. (2002) Identification of ter94, *Drosophila* VCP, as a modulator of polyglutamine-induced neurodegeneration. *Cell Death Differ.*, **9**, 264–273.
35. Ishigaki, S., Hishikawa, N., Niwa, J., Iemura, S., Natsume, T., Hori, S., Kakizuka, A., Tanaka, K. and Sobue, G. (2004) Physical and functional interaction between Dorfin and Valosin-containing protein that are colocalized in ubiquitylated inclusions in neurodegenerative disorders. *J. Biol. Chem.*, **279**, 51376–51385.
36. Kakizuka, A. (2008) Roles of VCP in human neurodegenerative disorders. *Biochem. Soc. Trans.*, **36**, 105–108.
37. Mizuno, Y., Hori, S., Kakizuka, A. and Okamoto, K. (2003) Vacuole-creating protein in neurodegenerative diseases in humans. *Neurosci. Lett.*, **343**, 77–80.
38. Marti, F. and King, P.D. (2005) The p95–100 kDa ligand of the T cell-specific adaptor (TSAd) protein Src-homology-2 (SH2) domain implicated in TSAd nuclear import is p97 Valosin-containing protein (VCP). *Immunol. Lett.*, **97**, 235–243.
39. Ju, J.S. and Weihl, C.C. (2010) p97/VCP at the intersection of the autophagy and the ubiquitin proteasome system. *Autophagy*, **6**, 283–285.
40. Ling, S.C., Albuquerque, C.P., Han, J.S., Lagier-Tourenne, C., Tokunaga, S., Zhou, H. and Cleveland, D.W. (2010) ALS-associated mutations in TDP-43 increase its stability and promote TDP-43 complexes with FUS/TLS. *Proc. Natl Acad. Sci. USA*, **107**, 13318–13323.
41. van Blitterswijk, M. and Landers, J.E. (2010) RNA processing pathways in amyotrophic lateral sclerosis. *Neurogenetics*, **11**, 275–290.
42. Kim, S.H., Shanware, N.P., Bowler, M.J. and Tibbetts, R.S. (2010) Amyotrophic lateral sclerosis-associated proteins TDP-43 and FUS/TLS function in a common biochemical complex to co-regulate HDAC6 mRNA. *J. Biol. Chem.*, **285**, 34097–34105.
43. Fiesel, F.C. and Kahle, P.J. (2011) TDP-43 and FUS/TLS: cellular functions and implications for neurodegeneration. *FEBS J.*, **278**, 3550–3568.
44. Ayala, Y.M., Zago, P., D'Ambrogio, A., Xu, Y.F., Petrucelli, L., Buratti, E. and Baralle, F.E. (2008) Structural determinants of the cellular localization and shuttling of TDP-43. *J. Cell Sci.*, **121**, 3778–3785.
45. Nagai, R., Hashimoto, R. and Yamaguchi, M. (2010) *Drosophila* Syntrophins are involved in locomotion and regulation of synaptic morphology. *Exp. Cell Res.*, **316**, 2313–2321.
46. Fernández-Sáiz, V. and Buchberger, A. (2010) Imbalances in p97 co-factor interactions in human proteinopathy. *EMBO Rep.*, **11**, 479–485.
47. Manno, A., Noguchi, M., Fukushi, J., Motohashi, Y. and Kakizuka, A. (2010) Enhanced ATPase activities as a primary defect of mutant valosin-containing proteins that cause inclusion body myopathy associated with Paget disease of bone and frontotemporal dementia. *Genes Cells*, **15**, 911–922.
48. Takahashi, Y., Hirose, F., Matsukage, A. and Yamaguchi, M. (1999) Identification of three conserved regions in the DREF transcription factors from *Drosophila melanogaster* and *Drosophila virilis*. *Nucleic Acids Res.*, **27**, 510–516.
49. Stewart, B.A., Atwood, H.L., Renger, J.J., Wang, J. and Wu, C.F. (1994) Improved stability of *Drosophila* larval neuromuscular preparations in haemolymph-like physiological solutions. *J. Comp. Physiol. A*, **175**, 179–191.
50. Ly, L.L., Suyari, O., Yoshioka, Y., Tue, N.T., Yoshida, H. and Yamaguchi, M. (2013) dNF-YB plays dual roles in cell death and cell differentiation during *Drosophila* eye development. *Gene*, **520**, 106–118.

EXPERIMENTAL CELL RESEARCH 326 (2014) 36–45

Available online at www.sciencedirect.com

ScienceDirect

journal homepage: www.elsevier.com/locate/yexcr

Research Article

Genetic link between Cabeza, a Drosophila homologue of Fused in Sarcoma (FUS), and the EGFR signaling pathway

Mai Shimamura[a,b,1], *Akane Kyotani*[a,b], *Yumiko Azuma*[c], *Hideki Yoshida*[a,b], *Thanh Binh Nguyen*[a,b], *Ikuko Mizuta*[c], *Tomokatsu Yoshida*[c], *Toshiki Mizuno*[c], *Masanori Nakagawa*[d], *Takahiko Tokuda*[c,e,**], *Masamitsu Yamaguchi*[a,b,*]

[a]*Department of Applied Biology, Kyoto Institute of Technology, Matsugasaki, Sakyo-ku, Kyoto 606-8585, Japan*
[b]*Insect Biomedical Research Center, Kyoto Institute of Technology, Matsugasaki, Sakyo-ku, Kyoto 606-8585, Japan*
[c]*Department of Neurology, Kyoto Prefectural University of Medicine, 465 Kajii-cho,Kamigyo-ku, Kyoto 602-8566, Japan*
[d]*North Medical Center, Kyoto Prefectural University of Medicine, 465 Kajii-cho, Kamigyo-ku, Kyoto 602-8566, Japan*
[e]*Department of Molecular Pathobiology of Brain Diseases, Graduate School of Medical Science, Kyoto Prefectural University of Medicine, 465 Kajii-cho, Kamigyo-ku, Kyoto 602-8566, Japan*

ARTICLE INFORMATION

Article Chronology:
Received 10 January 2014
Received in revised form
17 May 2014
Accepted 4 June 2014
Available online 11 June 2014

Keywords:
Amyotrophic lateral sclerosis
Cabeza
Retina
EGFR pathway
Drosophila

ABSTRACT

Amyotrophic Lateral Sclerosis (ALS) is a fatal neurodegenerative disease that causes progressive muscular weakness. Fused in Sarcoma (*FUS*) that has been identified in familial ALS is an RNA binding protein that is normally localized in the nucleus. However, its function in vivo is not fully understood. *Drosophila* has Cabeza (Caz) as a *FUS* homologue and specific knockdown of Caz in the eye imaginal disc and pupal retina using a *GMR-GAL4* driver was here found to induce an abnormal morphology of the adult compound eyes, a rough eye phenotype. This was partially suppressed by expression of the apoptosis inhibitor P35. Knockdown of Caz exerted no apparent effect on differentiation of photoreceptor cells. However, immunostaining with an antibody to Cut that marks cone cells revealed fusion of these and ommatidia of pupal retinae. These results indicate that Caz knockdown induces apoptosis and also inhibits differentiation of cone cells, resulting in abnormal eye morphology in adults. Mutation in EGFR pathway-related genes, such as *rhomboid-1*, *rhomboid-3* and mirror suppressed the rough eye phenotype induced by Caz

Abbreviations: Caz, Cabeza; ALS, Amyotrophic Lateral Sclerosis; *FUS*, Fused in Sarcoma; EGFR, Epidermal growth factor-receptor; SOD1, Cu/Zn superoxide dismutase; TDP-43, TAR DNA-binding protein of 43 kDa gene; CNS, central nervous system; APF, after pupal formation; ERK, Extracellular signal-related kinase.

*Corresponding author at: Department of Applied Biology, Kyoto Institute of Technology, Matsugasaki, Sakyo-ku, Kyoto 606–8585, Japan. Fax: +81 75 724 7799.

**Corresponding author at: Department of Molecular Pathobiology of Brain Diseases (Neurology), Graduate School of Medical Science, Kyoto Prefectural University of Medicine, 465 Kajii-cho, Kamigyo-ku, Kyoto 602–8566, Japan. Fax: +81 75 211 8645.

E-mail addresses: ttokuda@koto.kpu-m.ac.jp (T. Tokuda), myamaguc@kit.ac.jp (M. Yamaguchi).

[1] Present address: Environmental Research Laboratory of Public Health, Kankyo Eisei Yakuhin Co. Ltd., 3-6-2, Hikaridai, Seika-cho, Soraku-gun, Kyoto, Kyoto 619-0237, Japan

http://dx.doi.org/10.1016/j.yexcr.2014.06.004

knockdown. Moreover, the *rhomboid-1* mutation rescued the fusion of cone cells and ommatidia observed in Caz knockdown flies. The results suggest that Caz negatively regulates the EGFR signaling pathway required for determination of cone cell fate in *Drosophila*.

Introduction

Amyotrophic lateral sclerosis (ALS) is a fatal neurodegenerative disease that is characterized by degeneration of upper and lower motor neurons of the brain and the spinal cord, which leads to progressive muscle weakness and fatal paralysis [1]. Most cases of ALS are sporadic, but some patients have a familial history as a result of a mutation in the gene for Cu/Zn superoxide dismutase (SOD1) [2].

The family of MAPKs includes ERK, p38 and JNK. Each MAPK signaling pathway consists of at least three components, a MAPK kinase kinase, a MAPK kinase and a MAPK. Deviation from strict control of MAPK signaling pathways has been implicated in the development of human neurodegenerative diseases including Alzheimer's, Parkinson's and ALS [3]. Recently it was reported that aberrant expression and activation of p38 in motor neurons and microglia play important roles in ALS progression [4]. Persistent activation of p38 correlates with degeneration of motor neurons in transgenic mice expressing a mutant SOD1 [5,6]. Moreover a p38 inhibitor was demonstrated to prevent the apoptosis of motor neurons induced by a mutant SOD1 [7]. Thus a possible link between MAPK signaling and ALS has been suggested.

A substantial number of proteins linked to ALS are directly or indirectly involved in RNA processing [8]. Among RNA-binding proteins, mutations in the TAR DNA-binding protein of 43 kDa gene (*TDP-43*) and fused in sarcoma (*FUS*) gene have been identified as major genetic causes in both familial and sporadic ALS [9–18]. *TDP-43* and *FUS* are implicated in multiple aspects of RNA metabolism including transcriptional regulation, mRNA splicing and mRNA shuttling between the nucleus and the cytoplasm [19,20].

Drosophila has a single orthologue of human *FUS*, named Cabeza (*Caz*). In situ hybridization and immunohistochemistrical analyses demonstrated that *Caz* mRNA and protein are enriched in the brain and central nervous system (CNS) during embryogenesis, and the *Caz* protein has been detected in the nuclei of several larval tissues and in imaginal discs [21,22]. The full-length recombinant *Caz* protein and its RRM domain are capable of binding RNA in vitro [21]. These findings suggest that *Caz* is a nuclear RNA binding protein that may play an important role in the regulation of RNA metabolism during *Drosophila* development.

In our previous studies using neuron specific *Caz* knockdown flies, we demonstrated that *Caz* functions in neuronal cell bodies and/or axons of the CNS and is involved in elongation of synaptic branches of motoneurons [22]. However, contributions of *Caz* during development of various tissues in *Drosophila* are not fully understood. As a first step toward clarification, we investigated the effect of knockdown of *Caz* on eye development and revealed a rough eye phenotype, accompanied by apoptosis, abnormal differentiation of cone cells and defects in ommatidia rotation. In addition, a *Rhomboid-1* mutant could be shown to rescue the fusion of cone cells and mutations of *rhomboid-3* and *mirror* significantly suppressed the rough eye phenotype of the *Caz* knockdown flies. Since *rhomboid-1*, *rhomboid-3*, and *mirror* are EGFR pathway-related genes, these results indicate genetic links between *Caz* and EGFR signaling.

Materials and methods

Fly stocks

Fly stocks were maintained at 25 °C on standard food containing 0.7% agar, 5% glucose and 7% dry yeast. Canton S was used as the wild type. *w*; *UAS-Caz-IR*$_{363-399}$;+(CG3606) and *UAS-rho-IR*^{28690} was obtained from Vienna *Drosophila* RNAi Center (VDRC). The RNAi of this strain was targeted to the region corresponding to residues 363–399 of *Drosophila Caz* (*UAS-Caz-IR*$_{363-399}$). Four and seven transgenic strains carrying *UAS-Caz-IR*$_{1-167}$ and *UAS-Caz-IR*$_{180-346}$ were established [22]. Each transgenic strain showed a consistent phenotype. Alleles of the following genes were obtained from the Bloomington *Drosophila* stock center: *mirror*^{SaiD3}, *ru*^{1}, *rho*^{7M43} and *rho*^{AA69}. Enhancer trap lines carrying the lacZ markers AE127 (inserted into *seven-up*) [23] and *P82* (inserted into *deadpan*) [24] were obtained from Y. Hiromi and co- workers. These lines express the β-galactosidase marker in photoreceptor cells (R) of R3/R4/R1/R6 and R3/R4/R7. *hspFlp; +; tub*1> *FRT cd2 FRT> GAL4, UAS-GFP/ TM3* was a kind gift from A. Plessis. Establishment of lines carrying GMR-GAL4 was as described earlier [25]. Act5C-GAL4/ TM6B was also obtained from the Bloomington *Drosophila* stock center.

Generation of RNAi clones in retinae

RNAi clones in retinae were generated with the flip-out system [26]. Female flies with *hspFlp; +; tub*1> *FRT cd2 FRT> GAL4, UAS-GFP/ TM3* were crossed with *w; UAS-Caz-IR*$_{363-399}$;+male flies and clones were marked by the presence of GFP. Flip-out was induced 24–48 h after egg laying with a 60 min heat shock at 37 °C.

Immunostaining

For immunohistochemistory, larval eye imaginal discs and pupal retinae were dissected, and fixed in 4% paraformaldehyde/ PBS for 15 min and 30 min at 25 °C, respectively. After washing with PBS containing 0.3% Triton X-100, the samples were blocked with PBS containing 0.15% Triton X-100 and 10% normal goat serum for 30 min at 25 °C, and incubated with diluted primary antibodies in PBS containing 0.15% Triton X-100 and 10% normal goat serum for 16 h at 4 °C. The following antibodies were used; mouse anti-LacZ (1:500, Developmental Studies Hybridoma Bank [DSHB], 40-1a), mouse anti-Elav (1:200 DSHB 9F8A9), mouse anti-Cut (1:500, DSHB 2B10), mouse anti-Discs large (1:500) (DSHB) and anti-diphospho ERK (dpERK) (1: 500) (Sigma). After extensive washing

with PBS containing 0.3% Triton X-100, samples were incubated with secondary antibodies labeled with either Alexa 546 or Alexa 488 (1:400, Invitrogen) for 3 h at 25 °C. Alexa 488-conjugated phalloidin (200 units/ ml) was used for the detection of F-actin. After extensive washing with PBS containing 0.3% Triton X-100, samples were mounted in Vectashield (Vector Laboratories Inc.) and analyzed by confocal laser scanning microscopy (Olympus Flouview FV10i).

Western immunoblot analysis

Protein extracts from the whole pupae of *Drosophila* carrying *Act5C-GAL4/+* or *Act5C-GAL4/+*; *UAS-Caz-IR*$_{363-399}$/+ were prepared as previously described [22]. The homogenates were boiled at 100 °C for 5 min, and then centrifuged. The supernatants (extracts) were electrophoretically separated on SDS-polyacrylamide gels containing 12% acrylamide and then transferred to polyvinylidene difluoride (PVDF) membranes (Bio-Rad). The blotted membranes were blocked with TBS/0.05% Tween containing 5% skim milk for 1 h at 25 °C, followed by incubation with rabbit polyclonal anti-*Caz* at a 1:5,000 dilution for 16 h at 4 °C. After washing, the membranes were incubated with HRP-conjugated anti-rabbit IgG (GE Healthcare Bioscience) at 1:10,000 dilution for 2 h at 25 °C. Antibody binding was detected using ECL Western blotting detection reagents (GE Healthcare Bioscience) and images were analyzed using a Lumivision Pro HSII image analyzer (Aisin Seiki).

Apoptosis assay

Third instar larvae or 42APF pupae were dissected in PBS and the eye imaginal discs or pupal retinae were fixed in 4% paraformaldehyde in PBS for 30 min at 25 °C. After being washed with 0.3% PBST, the sample were permeabilized by incubation in 0.25% PBST for 20 min in 25 °C. After washing with H_2O, the TUNEL reaction was carried out using a Click-iT TUNEL Alexa Fluor 594 Imaging Assay Kit (Life Technologies) according to the manufacture's recommendations.

Scanning electron microscopy

Adult flies were anesthetized, mounted on stages, and observed under a scanning electron microscope (SEM) VE-7800 (Keyence Inc.) in the low vacuum mode. The eye phenotype of at least five adult male flies (3 to 5 days old) of each line was examined in each experiment and the experiments were done in triplicate. No significant variation in eye phenotype was observed among the five individuals.

Data analysis

Quantification of intensity of *Caz* signals was carried out with six to nine different samples by using Meta Morph software (Molecular Devices). For the statistical analysis, Microsoft Excel 2007 was used. *P*-values were calculated using Welch's *t*-test and the error bars represent Standard Errors from Means.

Results

Knockdown of *Caz* in eye imaginal discs induces morphologically aberrant rough eyes

In order to investigate in vivo functions of *Caz*, we examined the effect of reduction of *Caz* protein in vivo using a combination of the GAL4-UAS targeted expression system and the RNAi method. Knockdown of *Caz* in all tissues by the Act5C-GAL4 driver strain resulted in late pupal lethality in transgenic lines carrying *UAS-Caz-IR*$_{1-167}$ (data not shown). Knockdown of *Caz* in eye imaginal discs by the GMR-GAL4 driver strain, in which *Caz* double-stranded RNA (dsRNA) was expressed in the region posterior to the morphogenetic furrow, induced morphologically aberrant rough eyes. SEM images showed fusion of ommatidia and a lack of bristles (Fig. S1C–F). Flies carrying GMR-GAL4 alone exhibited apparently normal eye morphology (Fig. S1A, and B). Moreover, to eliminate the possibility of off-target effects, we established eleven independent transgenic fly lines carrying *UAS-Caz-IR* targeted to the different regions of the *Caz* mRNA assessed in a previous study [22]. Phenotypes of the established transgenic fly lines crossed with the GMR-GAL4 driver strain are reported [27]. Each independent strain showed the similar rough eye phenotype as the flies carrying *UAS-Caz-IR* targeted to different regions of the *Caz* mRNA (Fig. S1C–F). These results suggest that the rough eye phonotype observed in *Caz* knockdown flies is not due to a possible insertional mutation or off-target effect but rather to reduction of the *Caz* protein level. Throughout the following studies, we utilized the strain CG3606 carrying *UAS-Caz-IR*$_{363-399}$.

To investigate whether the expression of *Caz* dsRNA efficiently reduces the level of *Caz* protein, we performed immunostaining of pupal retinae for 42 h after pupal formation (APF) with anti-*Caz* antibodies. We utilized the flip-out system to produce the RNAi clone so that the level of *Caz* could be directly compared within a single retina. We used *UAS-Caz-IR*$_{363-399}$ line, since it apparently showed the severest rough eye (Fig. S1E and F). Within the RNAi clone of *Caz* marked by the presence of GFP signals, *Caz* signals marked by Red were reduced by 50% (Fig. 1A to G). Double immunostaining of pupal retinae with anti-cut antibody and ant-Caz antibody revealed relatively high expression of Caz in cone cells (Fig. 1J) and the Caz signal was reduced by 62% in flies expressing Caz dsRNA drived by *GMR-GAL4* (Fig. 1K and N). Moreover, effective knockdown of *Caz* in pupae of *UAS-Caz-IR*$_{363-399}$ line was demonstrated by the Western immunoblot analysis with anti-*Caz* antibody (Fig. 1O). All of these results further indicate that the rough eye phenotype observed in RNAi flies of *Caz* is due to reduction of the *Caz* protein level.

Knockdown of *Caz* induces apoptosis in pupal retinae

Extensive apoptosis could be considered as one factor causing fused ommatidia in the adult compound eye, since it is frequently accompanies this phenotype. We therefore examined if excessive cell death might occur during eye development in *Caz* knockdown flies by crossing *GMR-GAL4*; *UAS-Caz-IR*$_{363-399}$;+with flies expressing a broad specificity Caspase inhibitor P35 encoded by the baculovirus *Autographa californica* [28]. Partial suppression of the rough eye phenotype induced by knockdown of *Caz* was observed in flies co-expressing P35 (Fig. 2A, a–f). Expression of P35 alone

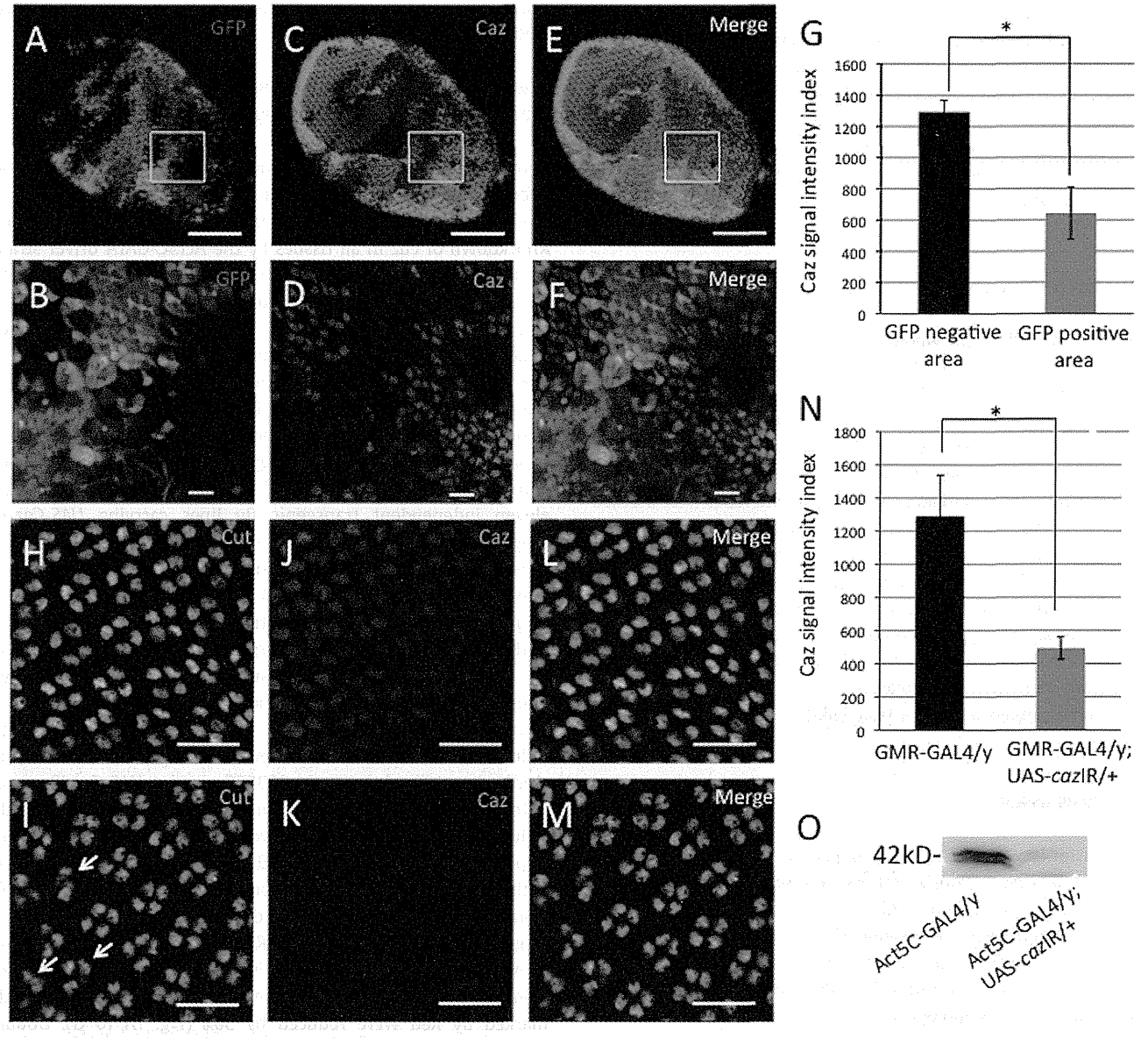

Fig. 1 – The level of anti-*Caz* signals is reduced in *Caz* dsRNA-expressing areas. Immunostaining of retinae for 42 h APF with anti-*Caz* antibody (C, D, J and K). RNAi clones in retinae were generated with the flip-out system (A to F). Female flies with *hspFlp; +; tub1>FRT cd2 FRT>GAL4, UAS-GFP* were crossed male flies with w; *UAS-Caz-IR*$_{363-399}$; +. The *Caz* dsRNA-expressing area is positively marked with GFP (A, and B). (E and F) Merged images. Panels B, D and F show higher magnification images of the regions marked with squares in panels A, C and D. (G) Quantification of intensities of *Caz*-signals in GFP-positive and –negative areas. Mean intensities with standard deviation from six pupal retinae are shown. *$P<0.05$. (H to M) Immunostaining of retinae for 42 h APF with anti-cut (H and I) and anti-*Caz* (J and K) antibodies. (L and M) Merged images. (H, J and K) *GMR-GAL4/y*. (I, K and M) *GMR-GAL4/y; UAS-Caz-IR*$_{363-399}$. (N) Quantification of intensities of *Caz*-signals. Mean intensities with standard deviation from nine pupal retinae are shown. *$P<0.05$. The bars indicate 100 μm (A, C and E), 10 μm (B, D and F) and 20 μm (H to M), respectively. (O) Western immunoblot analysis. Protein extracts were prepared from the whole pupae of *Drosophila* carrying *Act5C-GAL4/+* (left lane) or *Act5C-GAL4/+; UAS-Caz-IR*$_{363-399}$*/+* (right lane). The blot was probed with anti-*Caz* antibody.

exerted no apparent effect on the compound eye morphology (Fig. 2A, g and h). Moreover, we monitored apoptotic cells in third instar larval eye imaginal discs by TUNEL assay. However, no detectable apoptotic signals in eye imaginal discs of these flies was observed (Fig. 2B, a, d, g and j). We therefore next examined pupal retinae at 42 h APF by TUNEL assay. Apoptotic cells detected in the *Caz* knockdown retinae were significantly reduced in flies expressing P35 (Fig. 2B, c, f and i). These results indicate that knockdown of *Caz* induces apoptosis in some cells in pupal retinae.

Knockdown of *Caz* interferes with cell differentiation in pupal retinae

Photoreceptor cells are known to be generated in a stereotype order: R8 is generated first, with movement posterior from the

morphogenetic furrow, then cells are added pair wise (R2 and R5, R3 and R4, and R1 and R6), and R7 is the last photoreceptor to be added to each cluster [29]. To investigate whether *Caz* knockdown inhibits differentiation of photoreceptor cells, we crossed flies expressing *Caz* dsRNA with two enhancer trap lines, AE127 and P82, to specifically mark photoreceptor cells of R3/R4/R1/R6 and

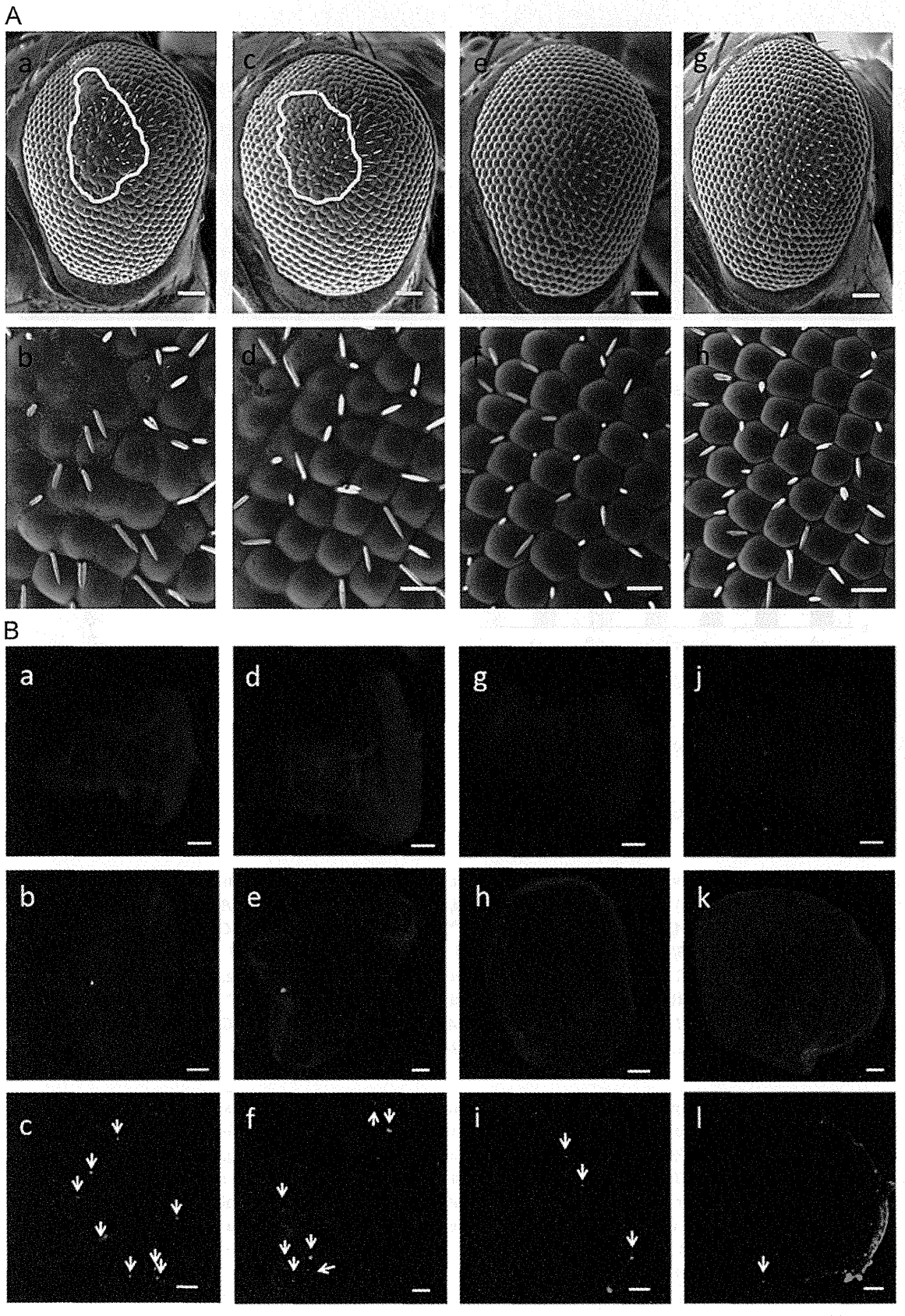

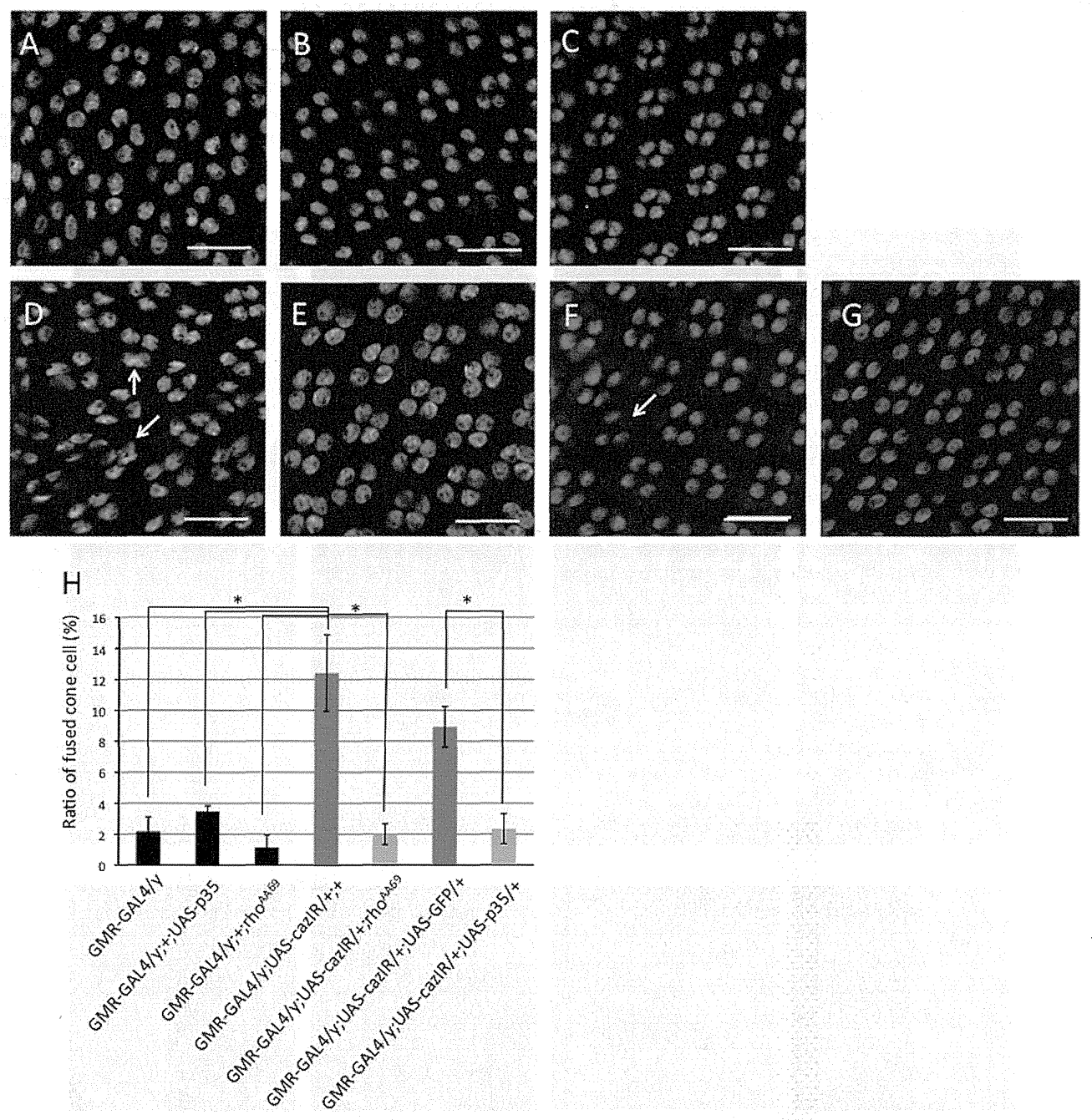

Fig. 3 – Knockdown of *Caz* interferes with differentiation of cone cells. Immunostaining of retinae for 42 h APF with an antibody to Cut that marks cone cells (green). (A) *GMR-GAL4/y*. (B) *GMR-GAL4/y*; +; *UAS-P35*/+. (C) *GMR-GAL4/y*; +; *rho*^{AA69}/+. (D) *GMR-GAL4/y; UAS-Caz-IR*$_{363-399}$/+; +. (E) *GMR-GAL4/y; UAS-Caz-IR*$_{363-399}$/+; *rho*^{AA69}/+. (F) *GMR-GAL4/y; UAS-Caz-IR*$_{363-399}$/+; *UAS-GFP*/+. (G) *GMR-GAL4/y; UAS-Caz-IR*$_{363-399}$/+; *UAS-P35*/+. The flies were developed at 28 °C. Arrows show fused cone cells and fused ommatidia are circled. The bar indicates 20 μm (A-G). (H) Quantification of fused cone cells in pupal retinae. Ratio of fused cone cells in each retina us shown (%). Mean values with standard deviation from six pupal retinae are shown. *$P<0.05$. (Left to Right) *GMR-GAL4/y, GMR-GAL4/y*; +; *UAS-P35*/+, *GMR-GAL4/y*; +; *rho*^{AA69}/+, *GMR-GAL4/y; UAS-Caz-IR*$_{363-399}$/+; +, *GMR-GAL4/y; UAS-Caz-IR*$_{363-399}$/+; *rho*^{AA69}/+, *GMR-GAL4/y; UAS-Caz-IR*$_{363-399}$/+; *UAS-GFP*/+ and *GMR-GAL4/y; UAS-Caz-IR*$_{363-399}$/+; *UAS-P35*/+.

Fig. 2 – Knockdown of *Caz* in eye imaginal discs induces apoptosis. (A) Over-expression of P35 suppresses the rough eye phenotype, as shown by scanning electron micrographs of adult compound eyes. (a, b) *GMR-GAL4/y; UAS-Caz-IR*$_{363-399}$/ +; +, (c, and d) *GMR-GAL4/y; UAS-Caz-IR*$_{363-399}$/+; *UAS-GFP*/+, (e, f) *GMR-GAL4/y; UAS-Caz-IR*$_{363-399}$/+; *UAS-P35*/+. (g, and h) *GMR-GAL4/y;* +/+; *UAS-P35*/ +. The flies were developed at 28 °C. The eye phenotype of at least five adult male flies (3 to 5 days old) of each line was examined and the experiments were done in triplicate. No significant variation in eye phenotype was observed among the five individuals. The rough area of the compound eye was circled as an index of the rough eye phenotype. The bars indicate 50 μm(a, c, e and g), and 14.2 μm(b, d, f and h), respectively. (B) Detection of apoptotic cells in third larval eye imaginal discs (a, d, g and j) and pupal retinae (c, f, i and l) by TUNEL assay. Pupal retinae were also stained with DAPI (b, e, h and k). (a to c) *GMR-GAL4/y; UAS-Caz-IR*$_{363-399}$/ +; +. (d to f) *GMR-GAL4/y; UAS-Caz-IR*$_{363-399}$/+; *UAS-GFP*/+. (g to i) *GMR-GAL4/y; UAS-Caz-IR*$_{363-399}$/+; *UAS-P35*/+. (j to l) *GMR-GAL4/y;* +/+; *UAS-P35*/+. The flies were developed at 28 °C. The bars indicate 100 μm.

R3/R4/R7, respectively and then immunostained the eye imaginal discs with anti-β-galactosidase antibodies (Fig. S2, A–B and D–E). In parallel, we carried out immunostaining of eye imaginal discs with anti-Elav antibodies (Fig. S2, C,and F). Elav, a pan-neuronal marker is normally expressed in the posterior portion of the eye imaginal discs. In eye imaginal discs of *Caz* knockdown flies, all eight photoreceptor cells and their neuron appeared to differentiate normally (Fig. S2).

We next examined the pattern formation in pupal ommatidia of *Caz* knockdown flies. Differentiation of photoreceptors, cone cells, and 1°, 2°, and 3° pigment cells was completed by about 42 h APF at 28 °C. However, in pupal retinae of *Caz* knockdown flies, immunostaining with an anti-Cut antibody that marks cone cells showed that some of these were fused in flies expressing *Caz* dsRNA (Fig. 3D and H). Flies carrying *GMR-GAL4* alone exhibited apparently normal cone cells (Fig. 3A and H). The quantified data indicate that occurrence of cone cell fusion was increased by 5.7 fold in the *Caz* knockdown retinae.

Furthermore, we monitored apical cell junctions in pupal retina for 42 h APF by immunostaining with anti-Discs large. The results showed cells in pupal retinae of *Caz* knockdown flies to be attached loosely, the orientation of ommatidia to be irregular, and the size of ommatidia to vary (Fig. 4C). In addition some ommatidia were apparently fused (Fig. 4C). These data suggest that knockdown of *Caz* disrupts differentiation of pupal ommatidial cell types, especially cone cells, and 1°, 2°, and 3° pigment cells, probably by repressing or enhancing expression of genes involved in differentiation processes.

Genetic link between *Caz* and *rhomboid*

The epidermal growth factor-receptor (EGFR) signaling pathway, evolutionarily conserved from *Caenorhabditis elegans* to man, controls a variety of different cellular processes. In *Drosophila*, these include proliferation, patterning, cell-fate determination, migration, and survival [30]. Contributions to cone cell-fate and ommatidial rotation have also been documented [30–33]. One of the rate limiting components of *Drosophila* EGFR signaling is *Rhomboid* [32–34]. We therefore examined the effects of mutations that might modify the Caz-induced rough eye phenotype, especially focusing on the *rhomboid* gene.

Half dose reduction *rhomboid-1* (*rho*) significantly suppressed the rough eye phenotype (Fig. 5A, a, b, c and d) and rescued the fusion of cone cells (Fig. 3E and H) in pupal retinae. Rescue of the fusion of the cone cells was also observed with overexpression of P35 (Fig. 3G and H), suggesting that induction of apoptosis is also responsible for this phenotype. Two different alleles of *rho* showed suppression of the rough eye (Fig. 5A, a, b, c and d). In addition, similar extent of suppression of the rough eye was observed by knockdown of *rho* (Fig. 5A, m and n), but not by expression of dsRNA for GFP (Fig. 5A, k and l). *Rhomboid-1* is a seven membrane-spanning serine protease, undergoing cleavage of Spitz to release the secreted form as an EGFR ligand from the Golgi apparatus [32–35]. In the eye, *Rhomboid-3*, also known as Roughoid, cooperates with *Rhomboid-1* [32,33]. Expectedly, the *Rhomboid-3* hypomorph mutant ru^1 also demonstrated suppression of the rough eye phenotype induced by knockdown of *Caz*

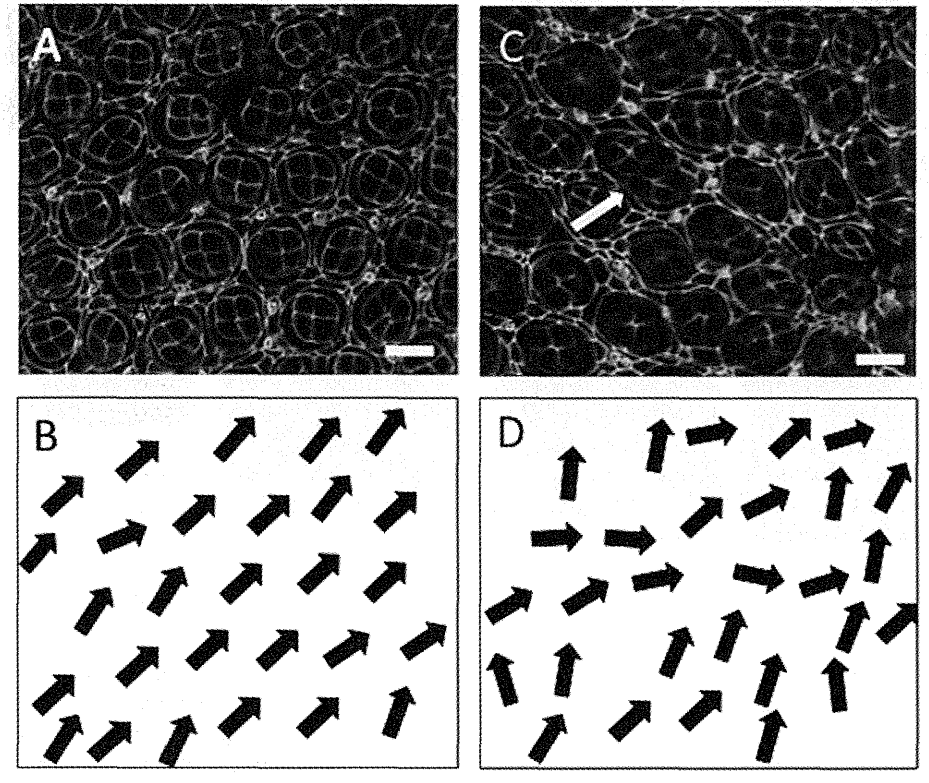

Fig. 4 – Effects of *Caz* knockdown on morphogenesis of pupal retinae. Confocal sections stained with anti-Discs large (A, and C). (A) *GMR-GAL4/y*. (C) *GMR-GAL4/y; UAS-Caz-IR*$_{363-399}$/+; +. Black arrows in the lower panels (B, and D) indicate the orientation of the ommatidia. Note disruption in the *Caz* knockdown flies (D) in compared to control (B). The size of ommatidia is also irregular, and cell attachment appears to be loose (compare panels A and C). The white arrow in panel C indicates an example of the fused ommatidia.

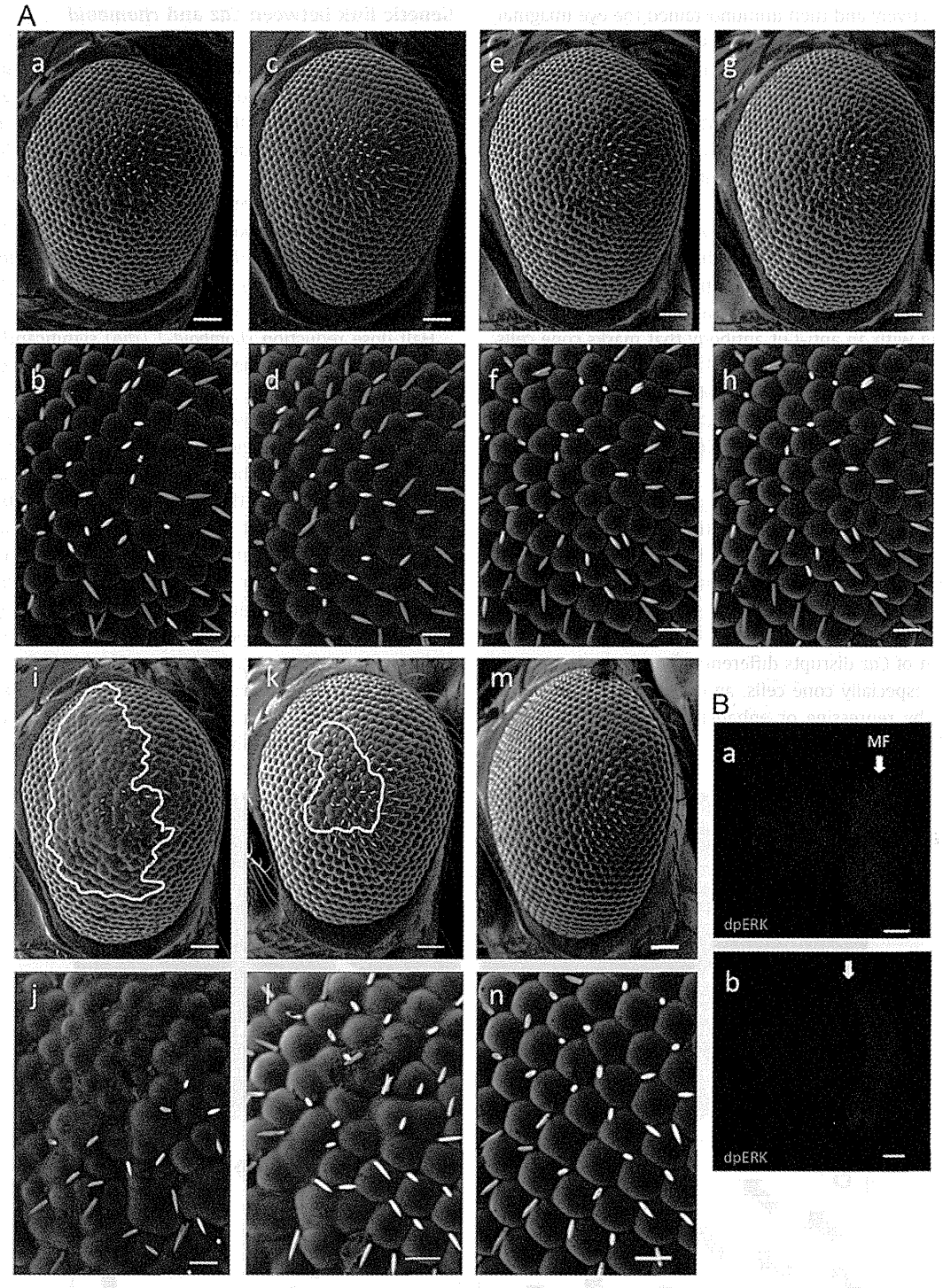

Fig. 5 – Scanning electron micrographs of adult compound eyes. (A) Female flies expressing *Caz* dsRNA (*GMR-GAL4/GMR-GAL4; UAS-Caz-IR*$_{363-399}$; +) were crossed with *UAS-GFP-IR, UAS-rho-IR*^{28690}, *rho*^{7M43} (amorph), *rho*^{4A69} (undetermined), *mirror*^{SaiD3} (loss of function), or *ru*^{1} (hypomorph) male flies, and then F1 progeny were developed at 28 °C without balancer chromosomes and used for inspection of the eye phenotype. The eye phenotype of at least five adult male flies (3 to 5 days old) of each line was examined and the experiments were done in triplicate. No significant variation in eye phenotype was observed among the five individuals. The rough area of the compound eye was circled as an index of the rough eye phenotype. (a, b) *GMR-GAL4/y; UAS-Caz-IR*$_{363-399}$/+; *rho*^{7M43}/+. (c, and d) *GMR-GAL4/y; UAS-Caz-IR*$_{363-399}$/+; *rho*^{4A69}/+. (e, and f) *GMR-GAL4/y; UAS-Caz-IR*$_{363-399}$/ +; *mirror*^{SaiD3}/+(g, and h) *GMR-GAL4/y; UAS-Caz-IR*$_{363-399}$/ +; *ru*^{1}/ +. (i, and j) *GMR-GAL4/ y; UAS-Caz-IR*$_{363-399}$/+; +. (k, and l) *GMR-GAL4/y; UAS-Caz-IR*$_{363-399}$/+; *UAS-GFP-IR*/+, (m, n) *GMR-GAL4/y; UAS-Caz-IR*$_{363-399}$/+; *UAS-rho-IR*^{28690}/+. The flies were developed at 28 °C. The bar indicates 50 μm (a, c, e, g, i, k, and m) or 14.2 μm (b, d, f, h, j, l, and n). (B) Immunostaining of eye imaginal discs with anti-dpERK antibody. (a) *GMR-GAL4/y.* (b) *GMR-GAL4/ y; UAS-Caz-IR*$_{363-399}$/+; +. Arrows indicate morphogenetic furrows (MF). The bars indicate 100 μm.